The role of TASK-2 channels in CO_2 sensing in zebrafish (*Danio rerio*)

Natalia Koudrina, B. Sc.

A thesis submitted to the
Faculty of Graduate and Postdoctoral Studies
in partial fulfillment of the requirements for the
Master's degree in Biology

Department of Biology
Faculty of Science
University of Ottawa

Abstract

Fish naturally experience fluctuating levels of O_2 and CO_2 in their environment. To cope with the deleterious effects of lowered O_2 (hypoxia) or elevated CO_2 (hypercapnia), fish exhibit an array of cardiorespiratory adjustments aimed at preserving homeostasis. One of the most significant of these responses is reflex hyperventilation. In zebrafish (*Danio rerio*), hyperventilation during hypoxia or hypercapnia is thought to be initiated by the activation of chemoreceptor cells, termed neuroepithelial cells (NECs) which detect changes in ambient levels of O_2 or CO_2. The NECs of larval zebrafish are found throughout the integument and recent studies have shown that these NECs likely mediate the ventilatory responses to hypoxia and the cardiac responses to hypercapnia. However, no study has yet examined the ventilatory response of larval zebrafish to hypercapnia and regardless of developmental stage, the signalling pathways involved in CO_2 sensing remain unclear. In the mouse, a background potassium channel (TASK-2) was shown to contribute to the sensitivity of chemoreceptor cells to CO_2. Zebrafish have two specific TASK-2 channel paralogs encoded by *kcnk5a* and *kcnk5b*. The purpose of this thesis was to determine whether TASK-2 channels are expressed in NECs of larval zebrafish and whether they are involved in CO_2 sensing. Immunohistochemical approaches were used to visualize TASK-2 protein (encoded by *kcnk5a*) within NECs of larvae and adult gill. TASK-2 protein was observed on NECs in both larvae and adult gill. Exposure of larvae to hypercapnia caused an increase in cardiac and breathing frequencies; these responses were blunted in fish experiencing either TASK-2 and/or TASK-2b knockdown. The results of these experiments suggest that TASK-2 has a role in activating NECs thus eliciting cardiorespiratory responses, when larvae are exposed to hypercapnia.

Résumé

Les poissons peuvent être exposés aux niveaux fluctuants d'O_2 et de CO_2 dans leur environnement. Pour surmonter les effets délétères d'une diminution de l'O_2 (hypoxie) ou du niveau élevé de CO_2 (hypercapnie), les poissons exhibent plusieurs ajustements cardiorespiratoires visant à préserver l'homéostasie. Un exemple de cet ajustement est le réflexe d'hyperventilation. Dans le poisson zèbre (*Danio rerio*), l'hyperventilation pendant l'hypoxie ou l'hypercapnie est initiée par l'activation des cellules chimioréceptrices appelées cellules neuroépithéliales (CNEs) qui détectent les changements dans le niveau ambiant d'O_2 ou de CO_2. Les CNEs de larves de poisson zèbre sont trouvés tout au long le tégument et les études récentes ont montré que ces CNEs peuvent assurer la médiation des réponses ventilatoires à l'hypoxie et les réponses cardiaques à l'hypercapnie. Néanmoins, aucune étude n'a examiné la réponse ventilatoire du poisson zèbre larvaire à l'hypercapnie quel que soit le stade de développement et les mécanismes de signalisation impliquées dans la détection du CO_2 n'est pas bien compris. Le canal potassique de fond (TASK-2) dans les souris contribue à la sensibilité des cellules chimioréceptrices au CO_2. Les poissons zèbres ont deux paralogues de canal TASK-2 codés par *kcnk5a* et *kcnk5b*. Le but de cette thèse est de déterminer si les canaux TASK-2 sont exprimés dans les CNEs de poisson zèbre larvaire et s'ils sont impliqués dans la détection du CO_2. L'immunohistochimie a été utilisée pour visualiser la protéine TASK-2 (codée par *kcnk5a*) dans les CNEs de larves et les branchies adultes. La protéine TASK-2 a été observée à la surface des CNEs dans les larves et les branchies adultes. Hypercapnie a augmenté la fréquence cardiaque et respiratoire aux larves. Ces réponses sont atténuées chez les poissons qui ont une perte de fonction de TASK-2 et/ou de TASK-2b. Les résultats de ces expériences suggèrent que TASK-2

a un rôle dans l'activation des CNEs, ce qui déclenche les réponses cardiorespiratoires lorsque les larves sont exposées à l'hypercapnie.

Acknowledgements

I would like to sincerely thank my two supervisors, Dr. Katie Gilmour and Dr. Steve Perry, for all their guidance, kindness, patience, and support throughout my Master's. Thank you for believing in me, right from the beginning, and giving me the chance to work with you. Your encouragement and valuable feedback has helped me improve in so many ways. I would also like to thank the members of my advisory committee, Dr. Marc Ekker and Dr. Michael Jonz for all of their assistance and suggestions. I am grateful to have had the opportunity to complete this research project.

Additionally, I would like to thank past and present Perry and Gilmour lab group members for their support, fun conversations, and assistance with experiments. I'm fairly certain that our prayers to the fish gods are what got us all through. A special thanks to Dr. Raymond Kwong and Dr. Villie Tzaneva for showing me the ropes and being patient while I learned all the important techniques. Both of you always took the time to answer even my silliest questions. A huge thank you to anyone who had gone out of their way to take care of my fish so I wouldn't have to bus to the lab for 2 hours on the weekend or a holiday. Carol Best, thank you for being a shoulder to lean on in my most difficult time. Jon Tea, thank you for translating my abstract even though it was last minute.

Thanks to Bill Fletcher, Vishal Saxena, Christine Archer and Andrew Ochalski for their help with experiments and animal care. Philip Pelletier, thank you for helping me with molecular techniques and answering all of my questions.

Last, but not least, I would like to thank my incredible family (including the cats) and Curtis Babineau for supporting me in every way through some of the toughest times of my life. All this would not be possible without them and I will be forever grateful for that.

Table of Contents

List of tables and figures

List of abbreviations

Abbreviation	Full name
°C	Degrees Celsius
5-HT	5-hydroxytryptamine or serotonin
AC	Adenylate cyclase
ANOVA	Analysis of variance
BCA	Bichinchoninic acid
bp	Base pair
BSA	Bovine serum albumin
CA	Carbonic Anhydrase
cDNA	Complementary deoxyribonucleic acid
DAPI	4’,6-diamidno-2- phenylindole
DEPC	Diethyl pyrocarbonate
DIG	Digoxygenin
DNA	Deoxyribonucleic acid
dNTP	Deoxynucleotide
dpf	Days post fertilization
EDTA	Ethylenediaminetetraacetic acid
f_H,	Heart rate
f_R,	Ventilation frequency
GPR	G protein-coupled receptor
h	Hour
hpf	Hours post fertilization

HRP	Horseradish-peroxidase
kDa	Kilodaltons
L	Litre
mg	Milligrams
min	Minutes
ml	Milliliter
mM	Millimolar
mmol	Millimole
mRNA	Messenger RNA
n	Sample size
nL	Nanoliter
NEC	Neuroepithelial cell
ng	Nanogram
$PaCO_2$	arterial blood carbon dioxide partial pressure
PBS	Phosphate-buffered saline
PBST	Phosphate-buffered saline-Tween
PCO_2	Carbon dioxide partial pressure
PCR	Polymerase chain reaction
PFA	Paraformaldehyde
PKA	Protein kinase A
PTU	1-phenyl-2-thiourea
PVDF	Polyvinylidene difluoride
RIPA	Radioimmunoprecipitation assay

RM	Repeated measures
RNA	Ribonucleic acid
RNase	Ribonuclease
RTN	Retrotrapezoid nucleus
RT-PCR	Reverse transcriptase-polymerase chain reaction
SDS	Sodium dodecyl sulfate
SDS-PAGE	Sodium dodecyl sulfate-polyacrylamide gel electrophoresis
SEM	Standard error of the mean
SSC	Saline-Sodium Citrate
T_a	Annealing temperature
TBST	Tris-buffered saline-Tween
V_m	Membrane potential
zn-12	Zebrafish neuron-specific surface antigen
µg	Microgram
µl	Microliter
µm	Micrometer
µmol	Micromoles

Chapter 1: Introduction

1.1 Overview

In aquatic environments, an increase in the partial pressure of carbon dioxide (PCO_2), termed hypercapnia, can negatively impact acid-base balance in teleost fish specifically by eliciting respiratory acidosis (a lowering of blood pH associated with the hydration of CO_2 to H^+ and HCO_3^-). Because the physiological effects of respiratory acidosis typically are deleterious, it is essential that fish are able to detect hypercapnia and thus initiate compensatory responses including cardiorespiratory adjustments. In mammals, the initiation of physiological responses to hypercapnia relies on the presence of chemoreceptors that detect changes in PCO_2 and/or pH (Lahiri and Forster, 2003). The primary peripheral chemoreceptors in mammals are the type I or glomus cells of the carotid body (Gonzalez et al., 1994; Lahiri and Forster, 2003), whereas fish use neuroepithelial cells (NECs) which are analogues to the type I cells and found on the skin of embryonic and larval fish and in the gill of juvenile and adult fish (Hockman et al., 2017).

Several lines of evidence suggest that cardiorespiratory responses during hypercapnia are initiated by NEC activation (Burleson and Smatresk, 2000; McKendry et al., 2001; Perry and Reid, 2002; Reid et al., 2000; Sundin et al., 2000). Initially, NECs were shown to act as O_2 chemoreceptors (Jonz et al., 2004; Zachar and Jonz, 2012). More recent evidence demonstrates that NECs also respond to changing levels of CO_2 (Abdallah et al., 2015; Qin et al., 2010). Although the cardiorespiratory responses of fish to elevated PCO_2 are well documented, the mechanism of activation of the NECs by hypercapnia remain poorly understood at the cellular level (Perry and Abdallah, 2012). Thus, the objective of the present study was to investigate the mechanisms underlying CO_2 sensing by zebrafish (*Danio rerio*) NECs by assessing the involvement of TASK-2 (acid-sensing) K^+ channels.

1.2 The cardiorespiratory response to hypercapnia

During exposure to environmental hypercapnia, a well-defined cardiorespiratory response is observed in adult fish. This response is comprised of increases in ventilation (hyperventilation), a lowering of heart rate (bradycardia) and increases in peripheral vascular resistance (reviewed by Gilmour, 2001; Gilmour and Perry, 2007; Perry and Abdallah, 2012; Sundin et al., 2007). Interestingly, teleost fish do not seem to display a comparable response to the elevation of internal PCO_2 (Gilmour et al., 2005; McKendry and Perry, 2001; see review by Gilmour and Perry, 2007), suggesting that chemosensors detect variation in water but not blood CO_2 tension.

Hyperventilation has been observed in most species that have been examined, although the sensitivity to CO_2 appears to vary widely among species (Gilmour, 2001; Gilmour and Perry, 2007). The hyperventilatory response consists of increases in breathing frequency and/or ventilatory stroke volume (Gilmour, 2001; Gilmour and Perry, 1994; Perry and Abdallah, 2012; Perry and Gilmour, 1996; Perry and Gilmour, 2002; Rantin et al., 1992; Soncini and Glass, 2000; Sundin et al., 2000). For example, tambaqui (*Colossoma macropomum*) responded to 5% CO_2 with increases in ventilation frequency but not amplitude (Sundin et al., 2000), although increases in both frequency and amplitude were observed at lower levels of CO_2 (Gilmour et al., 2005). Levels as low as 0.13% CO_2 caused an increase in ventilatory amplitude but not frequency in adult zebrafish (Vulesevic et al., 2006). Although the physiological benefit of hyperventilation in response to the elevation of environmental CO_2 levels has been debated, a consequence of this response is to lower arterial PCO_2 ($PaCO_2$) and thus raise blood pH for any given level of hypercapnia (Gilmour 2001; Perry and Abdallah, 2012).

Fewer species have been studied with respect to the cardiovascular responses to elevated CO_2 (e.g. McKendry et al., 2001; Perry and Mckendry, 2001; Perry et al., 1999; Reid et al., 2000; Sundin et al., 2000; reviewed by Perry and Gilmour 2002). Unlike the hyperventilation elicited by hypercapnia, which appears to be present in most species studied to date, bradycardia does not appear to be a universal response. For example, among adult fish, the white sturgeon (*Acipenser transmontanus*) displays the opposite response to hypercapnia, i.e. an increase in heart rate or tachycardia (Crocker et al., 2000). No response was observed in the American eel (*Anguilla rostra*) and brown bullhead (*Ameiurus nebulosus*), although this apparent lack of response may have reflected low sensitivity to CO_2 (Gilmour and Perry, 2007). The cardiovascular response to hypercapnia of adult zebrafish has not been reported to date, but zebrafish larvae responded to hypercapnia with tachycardia (Miller et al., 2014). In rainbow trout (*Oncorhynchus mykiss*), bradycardia is accompanied by an increase in systemic vascular resistance and hence hypertension (McKendry and Perry, 2001; Perry et al., 1999), but these vascular responses have been variable among the species examined, suggesting that there is no universal systemic vascular response to hypercapnia among fish (Perry and Gilmour, 2002).

1.3 Chemoreceptors and carbon dioxide sensing

Although the effects of CO_2 on ventilation in response to hypercapnia initially were thought to be indirect, mediated by the negative effects of hypercapnic acidosis on blood O_2 transport (Randall, 1982; Smith and Jones, 1982), it is now widely accepted that cardiorespiratory responses to hypercapnia are initiated by the activation of specialized sensory (chemoreceptor) cells (Jonz and Nurse, 2003; Gilmour and Perry 2007; Perry and Tzaneva,

2015). Studies that have examined the physiological responses to hypercapnia in mammals show that CO_2 sensing involves peripheral chemoreceptors (the type I cells of the carotid body; Lahiri and Forster, 2003; Peng et al., 2010). Central chemoreceptors in mammals are located within the brainstem, with the raphe nuclei and the retrotrapezoid nucleus (RTN) being specific areas that have been implicated in detecting changes in CO_2 (Gestreau et al., 2009; Guyenet et al., 2008; Severson et al., 2003). The carotid body is located near the bifurcation of the carotid artery and is highly vascularized. It contains glial-like type II cells that play an important physiological role in signalling in the carotid body, as well as the type I cells that are sensitive to changes in O_2 and CO_2 in arterial blood (Buckler, 2007; Nurse, 2014; Nurse and Piskuric, 2013). The carotid body is innervated by cranial nerves IX (glossopharyngeal) and X (vagus) which send signals to the central respiratory centre when glomus cells are stimulated by a rise in $PaCO_2$ (Kumar and Prabhakar, 2012). Animals with a denervated carotid body experience a significant delay between a hypercapnic stimulus and the resulting ventilatory response (Ahmad and Loeschcke, 1982; Smith et al., 2006).

In fish, which appear to lack central CO_2 chemoreceptors (at least in water-breathing fish; see Perry and Abdallah 2012), the peripheral CO_2 chemoreceptors are the NECs (Qin et al., 2010; Abdallah et al. 2015). NEC are located on the leading edge of the gill filament epithelial layer facing the incident water flow, placing them in an ideal location where water from the external environment can pass over the gills and changes in partial pressure can be detected (Perry and Tzaneva, 2016; Zachar and Jonz, 2012). CO_2 chemoreception was shown to be independent of changes in extracellular pH (Qin et al., 2010). Zebrafish NECs contain carbonic anhydrase (CA) and inhibition of CA caused a reduction in the depolarization response of isolated NECs to CO_2 at constant pH (isohydric hypercapnia; Qin et al., 2010) and blunted the

tachycardia response in larvae (Miller et al., 2014), suggesting that CO_2 sensing is mediated, at least in part, by a mechanism involving CA.

Although much remains to be learned about the cellular mechanisms of CO_2 sensing in NECs, it is likely that the broad brushstrokes of NEC activation resemble those of the homologous mammalian type I cells. Chemoreceptors are innervated and contain synaptic vesicles used for the storage and release of neurotransmitter (Cutz et al., 1993; Gonzalez et al., 1994; Kumar and Prabhakar, 2012; Ortega-Sáenz et al., 2013). Exposure to hypercapnia results in a rise in intracellular Ca^{2+} levels (Buckler and Vaughan-Jones, 1993; Kumar and Prabhakar, 2012) which triggers neurotransmitter release to afferent neurons (Buckler and Vaughan-Jones, 1994; Putnam et al., 2004; Sato, 1994). The increase in intracellular Ca^{2+} is mediated by a PKA-dependent mechanism (Summers et al., 2002). The current model for the activation of the L-type Ca^{2+} channels, located in type I cells of the carotid body, begins with elevated CO_2 levels (hypercapnia); the CO_2 is rapidly converted to H^+ and HCO_3^- (Lahiri and Forster, 2003). The elevation of HCO_3^- levels within the cell activates soluble adenylate cyclase (AC) which increases the levels of cAMP (Summers et al., 2002). The ensuing activation of protein kinase A (PKA) causes L-type Ca^{2+} channels to open causing increased chemoafferent discharge during increased PCO_2 and isohydric hypercapnia (Summers et al., 2002). In mammals, voltage-gated L-type Ca^{2+} channels allow extracellular Ca^{2+} entry into the cell (Buckler and Vaughan-Jones, 1994; Kumar and Prabhakar, 2012; Putnam et al., 2004; Summers et al., 2002).

1.3.1 NEC morphology and development

Dunel-Erb et al. (1982) first identified the NECs of the rainbow trout gill epithelium on the basis of their morphology, specifically the presence of dense-cored vesicles and positive

staining for serotonin (5-hydroxytryptamine or 5-HT). Subsequently, one or more populations of 5-HT-positive NECs have been found in all fish species studied to date, including zebrafish, rainbow trout, goldfish (*Carassius auratus*), several Amazonian teleosts, and bowfin (*Amia calva*; Coolidge et al., 2008; Jonz et al., 2004; Porteus et al., 2014; Saltys et al., 2006; reviewed by Perry and Tzaneva, 2015; Porteus et al., 2012). Moreover, NECs can sense hypoxia (Jonz et al., 2004), high levels of ammonia (Zhang et al., 2011), extracellular acidosis (Abdallah et al., 2015), and hypercapnia (Qin et al., 2010). In some species, such as goldfish and zebrafish, NECs are located primarily on the distal portion of the gill filament, while in others they are found scattered throughout the lamellae (Perry and Tzaneva, 2016). In both locations they are exposed to current flowing over the gill and therefore are conveniently located to detect changes in respiratory gases externally, i.e. in water. Because the filament NECs are in close proximity to the efferent filament artery, they are also well-placed to detect changes in respiratory gases internally, i.e. in arterial blood. The gill arches are innervated by both the IX^{th} and X^{th} cranial nerves (Reid et al., 2000; Sundin et al., 2000; reviewed by Milsom, 2002; Zachar and Jonz, 2012) and originate from the same embryonic tissue as the carotid body (Milsom, 2002; Zachar and Jonz, 2012). Similar to type I cells of the carotid body of mammals, which they resemble morphologically, NECs are innervated (Bailly et al., 1992; Jonz and Nurse, 2003; Saltys et al., 2006) and contain synaptic vesicles (80-100 nm diameter) enriched with neurochemicals such as serotonin (5-HT), endothelin, and enkephalins (Goniakowska-Witalińska et al., 1995; Perry et al., 2009; Porteus et al., 2012; Zaccone et al., 1989; Zaccone et al., 1992; Zaccone et al., 1997; Zaccone et al., 2006).

Although in adult fish the NECs that trigger cardiorespiratory responses to hypoxia and hypercapnia appear to be located exclusively in the gills and orobranchial cavity (Milsom et al.,

2002; Reid et al., 2000; Sundin et al., 2000), developing zebrafish exhibit responses to hypoxia even before the gills develop (Coccimiglio and Jonz, 2012; Jonz and Nurse, 2005). For example, a behavioural response to hypoxia was observed in zebrafish embryos at 2 days-post-fertilization (dpf; Jonz and Nurse, 2005) yet gill development only begins at 3 dpf with the appearance of gill filament primordia on the pharyngeal arches (Jonz and Nurse, 2005; Jonz and Nurse, 2006; Kimmel et al., 1995). At this stage, NECs are present on the gill arch (Jonz and Nurse, 2005). Once larvae reach 5 dpf, NECs develop on the gill filament, and these NECs become innervated at 7 dpf (Jonz and Nurse, 2006), with full gill development being reached at 14 dpf (Jonz and Nurse, 2005; Kimmel et al., 1995; Rombough, 2002). During early development, NECs are found on the integument of zebrafish larvae, appearing as early as 24-26 hours-post-fertilization (Coccimiglio and Jonz, 2012). Peak NEC density in the integument occurs at 3 dpf. After this developmental stage, there is a gradual reduction in skin NEC abundance corresponding to the increasing NEC population in the gills (Coccimiglio and Jonz, 2012). These integument NECs are thought to trigger the cardiorespiratory responses to hypoxia and hypercapnia that have been observed in developing zebrafish (Coccimiglio and Jonz, 2012; Jonz and Nurse, 2005; Miller et al., 2014).

1.3.2 CO_2 sensing by NECs

A sub-population of NECs in zebrafish has been demonstrated to sense both hypoxia and hypercapnia (Qin et al., 2010), a characteristic shared by the type I cells of the carotid body (Kumar and Bin-Jaliah, 2007). At the cellular level, zebrafish NECs respond to hypercapnia and hypoxia in a similar manner, with membrane depolarization (Jonz et al. 2004; Burleson et al. 2006; Qin et al., 2010). A rise in intracellular Ca^{2+} levels was documented in NECs exposed to

CO_2 (Abdallah et al., 2015). The Ca^{2+} responsible for this response was derived exclusively from intracellular storage compartments, with no contribution from extracellular Ca^{2+} sources, because the response was unaffected by the removal of extracellular Ca^{2+} or the use of Ca^{2+} channel blockers (Abdallah et al., 2015). The specific signal that triggers these responses remains equivocal, i.e. whether it is CO_2 or pH, and whether the cell is responsive to changes in the extracellular versus the intracellular compartment. Qin et al. (2010) reported that zebrafish NECs express CA and that inhibition of CA reduced the magnitude of the membrane depolarization and increased the time required to achieve the maximal response. In addition, typical responses to hypercapnia were detected when extracellular pH was held constant (i.e. isohydric hypercapnia). These results suggest that CO_2 detection does not require a change in extracellular pH, but rather relies on an intracellular sensor that responds to the rate of acidification associated with CA-catalyzed hydration of CO_2 (Qin et al., 2010). In agreement with this conclusion, inhibition of CA or CA knockdown using antisense oligonucleotide morpholinos resulted in a decreased reflex cardiovascular response to hypercapnia in zebrafish larvae (Miller et al., 2014). By contrast, the intracellular Ca^{2+} rise was independent of intracellular pH but required a change in extracellular pH (Abdallah et al., 2015). Specifically, the Ca^{2+} rise associated with acidic hypercapnia also could be elicited by extracellular acidosis in the absence of high CO_2 (i.e. isocapnic acidosis), but not by high CO_2 in the absence of a pH change (i.e. isohydric hypercapnia), nor by intracellular acidification alone induced by acetate (Abdallah et al., 2015). Similarly, although inhibition of CA attenuated changes in intracellular pH, it was without effect on the Ca^{2+} response (Abdallah et al., 2015). Collectively, this evidence suggests an uncoupling between membrane depolarization and changes in intracellular Ca^{2+}, a situation that remains to be resolved.

Membrane depolarization results from the inhibition of background K^+ channels (Qin et al., 2010). Specifically, NECs exhibited a CO_2-sensitive outwardly rectifying current that reversed near the equilibrium potential for potassium and that persisted when voltage-gated potassium channels were inhibited with 4-aminopyridine (Qin et al., 2010). However, sensitivity to hypercapnia was lost in the presence of the background K^+ channel blocker quinidine (Qin et al., 2010). Potassium channels that are sensitive to intracellular pH include inwardly rectifying K^+ channels (K_{ir}), Ca^{2+}-activated K^+ channels (K_{Ca}) and transient receptor potential (TRP) channels, all of which have been identified in mammalian type I cells and/or central CO_2-sensitive chemoreceptors (Hirata and Oku, 2010; Putnam et al., 2004). The findings of Abdallah et al. (2015) on the sensitivity of Ca^{2+} responses to extracellular pH suggest that potassium channels that are sensitive to extracellular H^+ also should be considered, and these include voltage-sensitive K^+ channels (K_V) and TWIK-related tandem pore domain acid-sensitive K^+ channels (TASK), both of which have been described in mammalian type I cells and/or central chemoreceptors (Buckler, 1999; Buckler, 2007; Putnam et al., 2004; Tan et al., 2007). Although the possibility that several types of K^+ channels are present in NECs (as well as mammalian glomus cells and central chemoreceptors) should not be ignored, K^+ channels that are members of the TASK family are attractive targets as the K^+ channels responsible for CO_2 sensing in NECs because they have been reported to be sensitive to CO_2 as well as both extracellular and intracellular pH (Peña-Münzenmayer et al., 2014). Fig. 1.1 outlines a proposed model for CO_2 sensing in NECs.

1.4 TASK channels

The early 1990s saw the cloning of members of all of the major K^+ channel families (i.e. voltage-gated, inwardly rectifying and Ca^{2+}-dependent), culminating in 1996 with the molecular identification of the two-pore or tandem pore domain K^+ channel (K_{2P}) family (Lesage et al., 1996). The members of this family, all of which are encoded by KCNK genes, are characterized by K^+ channel subunits that contain four transmembrane segments and two K^+ channel pore loop-forming domains; two K_{2P} subunits dimerize to form the functional channel containing the four pore loop topology that is characteristic of all known K^+ channels (Enyedi and Czirják, 2010). The K_{2P} structure is distinctive in that subunits of other K^+ channel families contain a single pore loop domain, with the functional channel involving a tetramer of subunits (Enyedi and Czirják, 2010). The distinctive K_{2P} topology and common electrophysiological features (i.e. a K^+-selective channel that is voltage-independent and shows Goldman-Hodgkin-Katz or open rectification) unify the members of this family, which is otherwise structurally diverse (Enyedi and Czirják, 2010). Reflecting this structural diversity, the fifteen members of the family identified to date in mammals were subdivided on the basis of sequence similarity into six subfamilies (Enyedi and Czirják, 2010). The first member of the family, cloned by Lesage et al. (1996), was named 'tandem of pore domains in a weak inward rectifying K^+ channel' or TWIK (K_{2P}1.1), with subsequent members of the family retaining similar nomenclature (Enyedi and Czirják, 2010; Goldstein et al., 2005). Of particular interest to the present study are a few members of the family that have been implicated in CO_2 sensing in central and/or peripheral mammalian chemoreceptors.

The TASK-1 (K_{2P}3.1) and TASK-3 (K_{2P}9.1) channels are members of the TWIK-related acid-sensitive K^+ (TASK) channel subfamily, which is characterized functionally by its sensitivity to extracellular pH, making these K^+ channels attractive targets for involvement in

CO_2 and pH chemosensing (Enyedi and Czirják, 2010). Although a number of studies reported that TASK-1 and TASK-3 were important for central chemoreception (Bayliss et al., 2001; Feldman et al., 2003; Lesage, 2003; Mulkey et al., 2004; Putnam et al., 2004; Talley et al., 2003; Washburn et al., 2002; Washburn et al., 2003), more recent work has not supported this conclusion (Enyedi and Czirják, 2010). In particular, the ventilatory response to changing CO_2 levels persisted in double knockout mice that lacked TASK-1 and TASK-3, therefore showing that these channels are not critical for central respiratory chemosensitivity (Mulkey et al., 2007). By contrast, several lines of evidence suggest that TASK-1 and TASK-3 located in the glomus cells of the carotid body have a role in the control of ventilation (Buckler, 2015; Enyedi and Czirják, 2010). The presence of TASK channels in glomus cells was suggested initially by the acid-sensitivity and pharmacological properties of the background K^+ current, and *in situ* hybridization confirmed the presence of TASK-1 mRNA in these cells (Buckler et al., 2000). More detailed characterization of the background K^+ current in glomus cells revealed properties similar to those of TASK-3 channels, leading to the suggestion, later confirmed, that glomus cells expressed heteromeric TASK-1/TASK-3 channels (Kim et al., 2009; Turner and Buckler, 2013; Williams and Buckler, 2004).

More recent work has focused on the role of TASK-2 ($K_{2P}5.1$), a TWIK-related alkaline pH activated K^+ (TALK) channel subfamily, in central CO_2/pH chemoreception (Guyenet et al., 2016). This channel has been observed to be expressed specifically in neurons of the CO_2/pH-chemosensitive RTN; these neurons exhibit a resting K^+ conductance that is inhibited by acidification, leading to membrane depolarization (Gestreau et al., 2010). In mice with a mutation of the transcription factor *phox2b*, the TASK-2 positive neurons of the RTN were lost and disruption of the respiratory chemoreflex leading to early mortality was observed. The

phox2b mutation in humans causes a congenital central hypoventilation syndrome, suggesting a role for TASK-2 in the control of ventilation (Gestreau et al., 2010). The generation of knockout mice lacking TASK-2 revealed that these animals were hypersensitive to low CO_2 concentrations (i.e. responded to lower than normal CO_2 levels) but exhibited a diminished ventilatory response at high levels of CO_2 (Gestreau et al., 2010). Moreover, RTN neurons from TASK-2 knockout mice showed reduced sensitivity to pH (44% did not respond to a change in pH) relative to RTN neurons from wild-type mice (<5% did not respond to a change in pH; (Wang et al., 2013). The variable responses of RTN neurons from TASK-2 knockout mice suggested that TASK-2 was not the only CO_2/pH-sensing pathway. Recently, the proton-activated G protein-coupled receptor GPR4 also was implicated in CO_2/pH sensing by RTN neurons (Kumar et al., 2015). In GPR4 knockout mice, responses to hypercapnia are reduced by 65% and can be restored by re-expression of GPR4 into RTN neurons (Guyenet et al., 2016; Kumar et al., 2015). Double knockout mice deficient in both GPR4 and TASK-2 exhibit a 90% reduction in the response to hypercapnia (Guyenet et al., 2016). Thus, GPR4 and TASK-2 appear to represent two independent cellular mechanisms for sensing pH.

A feature of TASK-2 that makes it particularly attractive as the cellular sensor of CO_2/pH in NECs is its sensitivity to both intracellular and extracellular pH (Cid et al., 2013; Lopez-Cayuqueo et al., 2015). Mammalian TASK-2 is closed by extracellular acidification in the range of physiological pH, and further activation occurs in response to alkalinisation (Reyes et al., 1998) , with arginine residue R224 serving as the sensor of extracellular pH (Niemeyer et al., 2007). The placement of this arginine residue on the extracellular surface of a transmembrane segment allows it to block the channel when it is protonated; at alkaline pH, deprotonation of R224 makes the channel available (Niemeyer et al., 2007). Furthermore, the effects of

intracellular pH on TASK-2 resemble those of extracellular pH, with acidification decreasing the K^+ current and alkalinisation increasing it (Niemeyer et al., 2010). Lysine 245 was shown to be the specific sensor for intracellular pH, a mechanism that was independent of that for extracellular pH (Niemeyer et al., 2010). Recently, data from a study by Pena-Munzenmayer et al. (2014) suggested that CO_2 can inhibit TASK-2 channels directly. Use of strongly buffered solutions to eliminate change in intracellular pH and neutralization of lysine 245 showed that the effect of CO_2 was not connected to intracellular acidification (Peña-Münzenmayer et al., 2014). Thus, with direct sensitivity to CO_2 as well as to intracellular or extracellular acidification, TASK-2 provides multiple avenues for sensing changes in CO_2 levels (Niemeyer et al., 2010; Peña-Münzenmayer et al., 2014).

In zebrafish, two target sequences that are orthologues of mouse TASK-2 have been identified, TASK-2 and TASK-2b (Peña-Münzenmayer et al., 2014). The zebrafish TASK-2 and TASK-2b channels are encoded by *kcnk5a* and *kcnk5b*, respectively. At the mRNA level, the identity between the two zebrafish sequences, which are probably paralogues, is 46%, increasing to 68.3% if only amino acids 1-240, a region that contains the sequence encoding for the transmembrane domain and the two pore segments, is taken into consideration (Peña-Münzenmayer et al., 2014). The identity between the mouse and zebrafish TASK-2 orthologues is 49.4% and increases to 73.3% at the amino acid level for the region encompassing amino acids 1-240. The same comparison performed with the second paralogue, TASK-2b, yielded identities of 40.7% and 64.6%, respectively (Peña-Münzenmayer et al., 2014). Only the function of TASK-2 was explored, by expressing TASK-2 in human embryonic kidney (HEK-293) cells. These experiments revealed that zebrafish TASK-2 exhibited properties comparable to those of mouse TASK-2, including inhibition by acidification and activation by alkalinisation for both

extracellular and intracellular pH, and inhibition by increasing CO_2 that included a direct effect of CO_2 (Peña-Münzenmayer et al., 2014). Notably, whereas the dependence of zebrafish TASK-2 on intracellular pH resembled that of mouse TASK-2, the dependence of zebrafish TASK-2 on extracellular pH was shifted to a more alkaline pH than was the case for mouse TASK-2, with the magnitude of the effect resembling the difference in systemic pH between fish and mammals (Peña-Münzenmayer et al., 2014). These characteristics suggest that zebrafish TASK-2 (and TASK-2b) warrant investigation as a mechanism of CO_2 sensing in NECs.

1.5 Hypothesis

The main objective of the present study was to test the hypothesis that TASK-2 and/or TASK-2b background K^+ channels play a role in CO_2 sensing in zebrafish (*Danio rerio*). If TASK-2 and/or TASK-2b play a role in CO_2 sensing in zebrafish, then these channels would be predicted to be localized to NECs and the loss of TASK channels would be predicted to impair cardiorespiratory responses to hypercapnia. These predictions were examined in 4 dpf zebrafish larvae, a developmental time point at which NECs remain abundant in the integument, and reliable cardiac (Miller et al., 2014) and functional knockdown using antisense oligonucleotide morpholinos is still effective.

Figure 1.1: Proposed model for CO_2 sensing in neuroepithelial cells (NEC). (1) CO_2 enters the cell and is hydrated into HCO_3^- and H^+, a reaction catalyzed by cytosolic carbonic anhydrase (CAc). (2) The pH within the cell decreases and causes a background K^+ channel to close, which (3) causes depolarization of the NEC and (4) release of Ca^{2+} from intracellular stores. Increased cytosolic Ca^{2+} activates the release of neurotransmitter. Figure modified from Perry et al., 2009; Carrie and Gilmour, 2012.

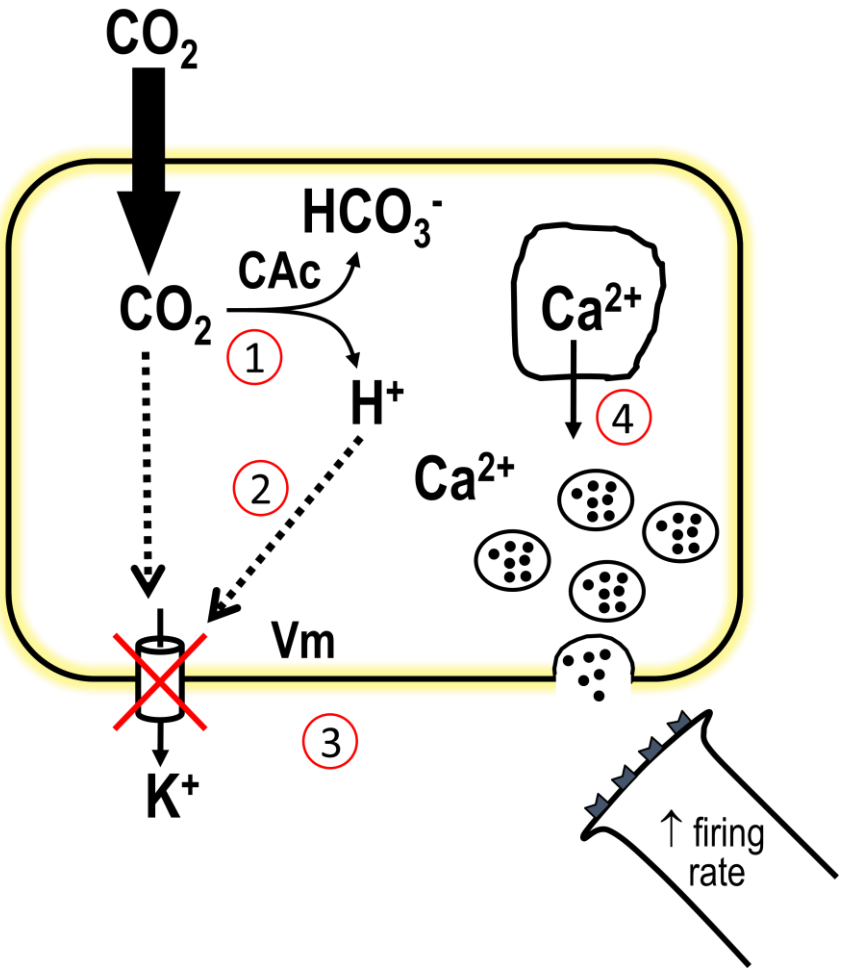
CO_2
HCO_3^-
CAc
CO_2
1
H^+
Ca^{2+}
4
2
Ca^{2+}
Vm
3
K^+
↑ firing rate

Chapter 2: Materials and Methods

2.1 Zebrafish husbandry

Mature wild-type zebrafish *(Danio rerio)* were obtained from the in-house breeding program at the University of Ottawa aquatic facility and held in 10 L acrylic tanks in re-circulating, flow-through aquatic housing systems (Aquatic Habitats, Apopka, FL, USA). The tanks were exposed to a 14h:10h light:dark cycle and supplied with aerated, dechloraminated city of Ottawa tap water at 28°C. Fish were fed twice a day with equal amounts of three diets: Zeigler Zebrafish, Golden Pearls (300-500 micron), and Zeigler AP100 5 (250-400 micron). For breeding, one male and two female adult fish were placed in a 2 L tank, separated by a divider (Westerfield, 2000). After an overnight acclimation period, the water in the tank was changed and the divider was removed to allow spawning. A fine mesh net was used to collect the embryos, which were placed in a 50 mL Petri dish containing E3 embryo medium (0.33 mM $CaCl_2 \cdot 2H_2O$, 0.17 mM KCl, 0.33 mM $MgSO_4 \cdot 6H_2O$, 5 mM NaCl, 0.0001% methylene blue) at a density of 60 embryos per dish. Embryos were held in an incubator kept at 28°C and embryo medium was changed daily until the fish were used for experiments at 4 dpf. Because larvae were used for experiments at 4 dpf, they were not fed. All procedures were conducted in compliance with University of Ottawa institutional guidelines, were approved by the Animal Care Committee (protocol BL-226), and were in accordance with the guidelines of the Canadian Council on Animal Care for the use of animals in research and teaching.

2.2 Localization of *kcnk5a*/TASK-2 and *kcnk5b*/TASK-2b

2.2.1 Analysis of mRNA expression by RT-PCR

Twenty larvae were pooled as a sample (n = 1), euthanized in a buffered solution of MS-222 (0.72 mg mL^{-1} 3-aminobenzoic acid ethyl ester; 21 mM Tris, pH 7; Sigma-Aldrich, St. Louis, MO, USA; Westerfield, 2000) and flash frozen in liquid nitrogen before being stored at -80°C. Adult zebrafish were euthanized individually as described above, and all gill arches were dissected from a fish (n = 1). Gill tissue was flash frozen in liquid nitrogen before being stored at -80°C. Larvae and adult gill tissue were homogenized using a pestle grinder (Kimble Chase Kontes, Rockwood, TN, USA). To avoid sample contamination, a separate autoclaved pestle was used for each sample. Total RNA was extracted using the RNeasy Mini Kit (Qiagen, Toronto, ON, Canada) according to the manufacturer's protocol. Extracted RNA was quantified using a NanoDrop® ND-1000 UV-Vis Spectrophotometer (ThermoFisher Scientific, Ottawa, ON, Canada). Following the manufacturer's protocol, cDNA was synthesized from 1 µg of RNA using the QuantiTect Reverse Transcription Kit (Qiagen).

Exon-spanning primers (Table 2.1) were designed for zebrafish *kcnk5a* and *kcnk5b* using Primer Quest® (IDT, Kanata, ON, Canada) and primer quality was assessed using OligoAnalyzer 3.1 (IDT). Primer specificity was confirmed by sequencing RT-PCR products (DNA sequencing facility at the Ottawa Hospital Research Institute). All PCR reactions were carried out using a Bio-Rad S1000 Thermal Cycler (Bio-Rad, Mississauga, ON, Canada) set for denaturation at 95ºC (30 s) and extension at 72ºC (45 s). The annealing temperature (T_a) and the number of cycles used for specific primer sets are outlined in Table 2.1. Each PCR reaction consisted of 200 ng of template cDNA, 2 µL of 10X DreamTaq buffer (ThermoFisher Scientific), 0.4 µL of 10 µmol L^{-1} dNTPs (Life Technologies, Burlington, ON, Canada), 0.4 µL of each forward and reverse primer (10 µmol L^{-1}) and 0.1 µL of DreamTaq DNA polymerase

(ThermoFisher Scientific) made up to 20 µL total volume with autoclaved water. The sizes of PCR products were determined by gel electrophoresis using 2% agarose (Life Technologies) gels containing RedSafe Nucleic Acid Staining Solution (iNtRON Biotechnology, Korea). Gels were cast using molds from Owl Separation systems (Portsmouth, NH USA). A 100 bp DNA ladder RTU (Ready-To-Use; GeneDireX, Nevada, USA) was run with the samples to determine the size of the amplicons.

2.2.2 Localization of mRNA by in situ hybridization

The template used to generate a probe against *kcnk5a* was a PCR product, synthesized from commercially-available bacterial non-expression plasmids (GE Healthcare Dharmacon Inc, USA), containing the open reading frame for *kcnk5a (ID:* MDR1734-202796179*)*. Open reading frame orientation and sequence within the plasmid were confirmed with sequencing. The exon-spanning primers for *kcnk5a* (Table 2.1) were modified by the addition of a T7 RNA polymerase start sequence (Table 2.2). All PCR reactions were carried out as described above and product sizes were verified by gel electrophoresis. The resulting PCR product was purified using the QIAquick® PCR purification kit (Qiagen) according to the manufacturer's protocol and used as a template for *in vitro* transcription with T7 RNA polymerase to create the antisense and sense riboprobes. The *in vitro* transcription reaction consisted of 400 ng of template (purified PCR product), 2 µL of 10X transcription buffer (Roche, Laval, QC), 2 µL of 10X digoxygenin (DIG) RNA labelling mix (Roche), 1 µL of RNase out recombinant ribonuclease inhibitor (Life technologies), and 2 µL of T7 RNA polymerase (Roche) made up to 20 µL total volume with RNase-free water. The reaction mixture was incubated at 37ºC for 4 h. Following the incubation, Turbo DNase (1 µL; Life technologies) was added and the reaction was incubated for an

additional 15 min at 37ºC. To precipitate RNA, 30 µL of LiCl (Life Technologies) were added to the reaction mixture and it was stored overnight at -20ºC. The following day, the reaction was centrifuged at 16,000 *g* at 4ºC for 15 min. The resulting pellet was washed with 1 mL of 70% EtOH in diethyl pyrocarbonate (DEPC) H_2O and re-centrifuged. The supernatant was removed and the pellet was dried for 10 min on ice before being resuspended in RNase-free water. The sizes of the sense and antisense riboprobes were confirmed by gel electrophoresis as described above. It should be noted that similar techniques were used in an attempt to generate a riboprobe against *kcnk5b* but technical problems were encountered.

To prepare samples for *in situ* hybridization, larvae were treated with 0.0045% 1-phenyl-2-thiourea (PTU; Sigma-Aldrich) starting at 24 hpf and continuing until sampling at 4 dpf. Larvae were terminally euthanized as described above and fixed in 4% paraformaldehyde (PFA; Santa Cruz Biotechnology, Santa Cruz, CA, USA) overnight at 4ºC. The fixed larvae were rinsed with phosphate-buffered saline containing 0.1% Tween-20 (PBST), immersed in a 30% sucrose solution at 4ºC overnight, and embedded in Cryomatrix (Shandon Cryomatrix, ThermoFisher Scientific, Burlington, ON). Tissue sections (10 µm) were obtained using a cryostat (Leica CM3050S; Concord, ON), and mounted on Superfrost® Plus microscope slides (ThermoFisher Scientific).

Slides were incubated overnight with either the sense or antisense probe in a humidified chamber at 65ºC. The riboprobe (400 ng) was diluted in hybridization buffer consisting of 50% deionized formamide (BioShop, Burlington, ON, Canada), 5X sodium chloride and sodium citrate solution (SSC), 0.1% Tween-20, 9.2 mmol L^{-1} citric acid (pH 6), 50 µg mL^{-1} heparin (Sigma-Aldrich), and 500 µg mL^{-1} yeast transfer-RNA (Invitrogen). Slides were washed 2x 30 min at 65ºC with hybridization buffer and 2x 30 min at room temperature with PBST. In a

humidified chamber, slides were incubated for 60 min at room temperature in a blocking solution of 10% bovine serum concentrate (BSC) in PBST. The blocking solution was then replaced with fresh 10% BSC containing an alkaline phosphatase-conjugated anti-DIG antibody at a 1:1000 dilution (Roche). The slides were incubated overnight at 4ºC then washed 5x 20 min in PBST and 2x 10 min in alkaline Tris buffer (100 mmol L^{-1} NaCl, 100 mmol L^{-1} Tris HCl at pH 9.5, 50 mmol L^{-1} $MgCl_2$, and 0.1 % Tween-20). Finally, the slides were incubated in a humidified chamber in the dark at room temperature with a staining solution consisting of nitroblue tetrazolium chloride (Sigma-Aldrich) and 5-bromo-4-chloro-3-indolylphosphate p-toluidine salt (ThermoFisher Scientific; Rockford, IL). Once the desired colour intensity was achieved, the slides were washed 3x 5 min in distilled water and fixed in 4% PFA for 20 min to stop the colour reaction. After *in situ* hybridization, the slides were cover-slipped and imaged using an Olympus CX41 microscope.

2.2.3 Localization of TASK-2 and TASK-2b protein by immunohistochemistry

Custom rabbit polyclonal antibodies (GenScript, USA) raised against zebrafish TASK-2 and TASK-2b were generated using synthetic peptide antigens. For TASK-2, the synthetic peptide CSDHGQSYERLVEEY corresponding to amino acids 492 to 506 of the zebrafish protein sequence (NP_001032478.1) was used. For TASK-2b, the synthetic peptide CVSEDRSLGKRSFG corresponded to amino acids 435 to 449 of the zebrafish protein sequence (NP_956927.1). The specificity of the resultant antibodies was examined by western blotting. A sample consisting of 30 4-dpf larvae was homogenized using a pestle grinder (Kimble Chase Kontes) in 150 µL of RIPA buffer (150 mM NaCl, 1% Triton-X 100, 0.5% sodium deoxycholate, 0.1% sodium dodecyl sulphate (SDS), 50 mM Tris-HCl, 1 mM 2,2',2",2"'-(ethane-

1,2-diyldinitrilo) tetraacetic acid (EDTA), 1 mM phenylmethanesulphonyl fluoride) containing a protease inhibitor cocktail (Roche). Extracted protein was mixed with an equal volume of Laemmli sample buffer (Sigma-Aldrich) and heated for 10 min at 65°C. Proteins were size-separated using a 12% SDS-PAGE gel and transferred to a polyvinylidene difluoride (PVDF) membrane via a semi-dry Trans-Blot SD transfer system (Bio-Rad). The membrane was incubated with 5% skim milk powder in TBST (20 mM Tris-HCl, 300 mM NaCl, 0.1% Tween 20, 0.02% sodium azide, pH 7.5) for 1 h at room temperature on a shaker and then probed overnight at 4°C with the TASK-2 (1:1000) or TASK-2b (1:250) antibody in 2% skim milk solution in TBST. Membranes were then rinsed 3x for 5 min each time in TBST and incubated with a 1:5000 dilution (in TBST) of horseradish-peroxidase (HRP) goat anti-rabbit IgG (Pierce, Rockford, IL, USA) for 2 h at room temperature. After a final wash in TBST (3x 15 min), bands were detected using Luminata Classico Western HRP substrates (Millipore, ThermoFisher Scientific). For TASK-2, the predicted protein size is 58 kDa and a band was observed at 56 kDa (Fig. 2.1). This band was not present in pre-immune serum. The same band was eliminated by pre-incubation of the antibody with the peptide against which it was raised (Fig. 2.1). For TASK-2b, the predicted protein size is 50.8 kDa and a band was observed at 50.6 kDa (Fig. 2.1). Again, the band was not present in pre-immune serum and was eliminated by pre-incubation of the antibody with the peptide against which it was raised (Fig. 2.1).

For immunohistochemistry using the custom TASK-2 and TASK-2b antibodies, larvae were euthanized by immersion in a buffered solution of MS-222 as described above, and fixed overnight at 4°C in 4% PFA. The fixed larvae were washed 5x with PBST and incubated for 5 min at room temperature in 50% MeOH followed by 100% MeOH. After 24 h at -20°C, larvae were rehydrated by immersion in 50% MeOH for 5 min followed by five washes with PBST.

Antigen retrieval was enhanced by incubation in 150 mM tris-HCl (pH 9.0) for 10 min at room temperature followed by 15 min at 65°C. After washing in PBST, larvae were incubated for 24 h at 4°C in blocking solution (0.8% Triton-X 100 and 2% bovine serum albumin (BSA) dissolved in PBS), and then with primary antibodies (Table 2.3) overnight at 4°C on a shaker. Subsequently, samples were rinsed 5x for 5 min each time with PBST, and incubated in the dark on a shaker for 1 h with the appropriate secondary antibodies (Table 2.3) in 0.8% Triton-X 100 in PBST solution. Finally, samples were rinsed 5x for 5 min with PBST and mounted with Vectashield mounting medium containing (4',6-diamidino-2-phenylindole (DAPI) (Vector Laboratories Inc. Burlingame, CA, USA) on a concave depression slide for imaging using a confocal laser scanning microscope (A1R+, Nikon Instruments, Melville, NY, USA). Image analysis was carried out using Nikon Elements software (Nikon Instruments).

2.3 Knockdown of TASK-2/*kcnk5a* and TASK-2b/*kcnk5b*

Antisense oligonucleotide morpholinos against *kcnk5a* and *kcnk5b* were used to achieve functional knockdown of TASK-2 and TASK-2b protein levels. Embryos were injected at the 1-2 cell stage of development with an antisense oligonucleotide (Gene Tools LLC, Philomath, OR, USA) designed to be complementary to either the translational start site, (*kcnk5a*; 5'-AGAGGTCCCTTGTCCACCATAATGA-3') or a splicing site (*kcnk5a*; 5'-TAACTGGACTTCATTCCTACCTCTA-3'; *kcnk5b*; 5'-CGCCACTACCTGTTGTTGAAACATA-3') (Fig. 2.2). The splice blocking morpholinos introduce a premature stop-codon, resulting in a truncated protein. Morpholinos were prepared to a final concentration of 4 ng nL^{-1} in 1X Danieau buffer (5.0 mmol L^{-1} HEPES (pH 7.6), 58 mmol

L^{-1} NaCl, 0.4 mmol L^{-1} $MgSO_4$, 0.6 mmol L^{-1} $Ca(NO_3)_2$, 0.7 mmol L^{-1} KCl) containing 0.05% (v/v) phenol red (as a visible indicator of successful injection); embryos were injected with 1 nL of this solution. To control for possible effects of microinjection, a separate group of 'sham' embryos was injected with 1 nL of a control morpholino (5'-CCTCTTACCTCAGTTACAATTTATA-3'; Gene Tools) prepared to the same final concentration. There is no known target sequence for this morpholino in zebrafish. Morphant and sham larvae were raised to 4 dpf for experimentation under the same conditions as described above.

2.3.1 Confirmation of knockdown

The effectiveness of knockdown was assessed by RT-PCR, western blotting and immunohistochemistry. For the splice-blocking morpholinos against *kcnk5a* and *kcnk5b*, RT-PCR was used to determine whether transcript size was altered in accordance with the expected effect of the antisense oligonucleotide (Fig. 2.2). The primers used for this purpose are listed in Table 2.1; RT-PCR was carried out as described above (see section 2.2.1). For *kcnk5a*, transcript abundance was quantified using exon-spanning *versus* intron-spanning primers (Table 2.1). The *kcnk5a* morpholino prevents splicing of the first intron (15 199 bp) which introduces a premature stop-codon. Owing to PCR limitations, the resulting, very large, PCR product cannot be detected but a reduction in abundance of the normal transcript, detected with exon-spanning primers, would be predicted to occur in morphants injected with the splice-blocking morpholino against *kcnk5a*. Intron-spanning primers were used as an additional method to detect knockdown because a band should only be detected in the *kcnk5a* morphants. The splice-blocking morpholino against *kcnk5b* was expected to result in the loss of an exon, leading to a reduction in

mRNA size (Fig. 2.2). The loss of an exon also causes a frame shift resulting in a premature stop codon. Band density quantification was carried out using ImageJ software, and *kcnk5a* mRNA expression was normalized to that of the V-type H^+-ATPase. Expression of H^+-ATPase was used for normalization because signal over-saturation was seen with the more commonly used β-actin. Signal over-saturation prevented accurate comparison of the sham and *kcnk5a* injected fish.

For western blotting, a sample consisting of 30 sham or morphant larvae was homogenized using a pestle grinder and proteins were extracted and prepared as described above. The total protein concentration of each sample was determined using a bicinchoninic acid (BCA; Sigma-Aldrich) assay with BSA as the standard. A serial dilution of protein samples was prepared to determine the appropriate loading amount for gel electrophoresis (Fig. 2.3). To keep protein levels within the linear dynamic range, 20 μg of protein were used for TASK-2 and 50 μg for TASK-2b (Taylor and Posch, 2014). Protein samples were separated based on size using a 12% SDS-PAGE gel for TASK-2b (as described above) or a 12% TGX Stain-Free FastCast Acrylamide gel (Bio-Rad) for TASK-2. Prior to sample transfer to PVDF membranes (carried out as described above), the stain-free gel was activated for 1 min with UV light to visualise total protein. Membranes were probed with the custom antibodies against TASK-2 (1:1000) or TASK-2b (1:250) as described above. To control for protein loading in western blots for TASK-2b, membranes were stripped with Re-Blot Plus solution (Millipore) used according to the manufacturer's instructions and re-probed with a 1:4000 dilution of anti-β-actin (A2066, Sigma-Aldrich). Band density quantification was carried out using ImageLab software (Bio-Rad, USA). For TASK-2, protein abundance was normalized against total protein whereas for TASK-2b, protein abundance was normalized against ß-actin protein abundance. Immunohistochemistry

using the TASK-2 antibody was carried out as a qualitative method of confirming knockdown. Immunohistochemistry was performed as described above (section 2.2.3).

2.4 Measurement of heart rate (f_H) and ventilation frequency (f_R)

To evaluate the roles of TASK-2 and TASK-2b in the detection of CO_2 by NECs, heart rate (f_H) and ventilation frequency (f_R) responses to hypercapnia were assessed in 4 dpf sham and morphant larvae. Exposure to hypercapnia in combination with adrenaline or hypoxia was used to test the capacity for heart rate and ventilation frequency responses. The experimental approach used was essentially that described by Miller et al. (2014). In brief, a larva was anaesthetized in 0.06 mg mL^{-1} Tris-buffered MS-222 and transferred to a temperature-controlled flow-through chamber perfused with the same anaesthetic solution gravity-fed from a reservoir through gas-impermeable tubing (Tygon, Saint-Gobain Performance Plastics, Pittsburgh, PA, USA). All trials were performed at 28°C with a flow rate of 125 mL h^{-1}; solution was removed from the chamber using a peristaltic pump (ThermoFisher Scientific). Breathing and heart rate were recorded using a video camera (3CCD camera, Dage-MTI, USA) mounted on a dissecting microscope (CMZ1500, Nikon) and connected to a computer. Videos were captured using CyberLink Power Director Software (Santa Clara, CA, USA).

Each larva was exposed to normoxic, normocapnic conditions for a 20 min acclimation and control period. Baseline heart rate and ventilation frequency measurements were collected for the last 2 min of this control period. Heart rate and ventilation frequency measurements were collected by visual assessment of, respectively, heart and mouth or opercular movements from the video recordings. Larvae that did not breathe at least once during the control period were

eliminated from further testing. The larva was then exposed to 1.5% CO_2 in air (hypercapnia) for 30 min. This level of hypercapnia was chosen based on pilot trials in which it reliably evoked a response; Miller et al. (2014) reported that 4 dpf larvae did not respond to lower levels of hypercapnia (0.25-0.75% CO_2). The CO_2 level in the perfusate reservoir was adjusted using an in-house custom-built gas mixer based on digital mass flow controllers, which provided mixed gas to the reservoir at a rate of 1000 ccm. Finally, the larva was exposed for 30 min either to a combination of 1.5% CO_2 and hypoxia (30 Torr, achieved by equilibrating the perfusate reservoir with a gas mixture containing 85% N_2, 1.5% CO_2, balance air) or to a combination of 1.5% CO_2 and 10^{-4} mol L^{-1} adrenaline (general adrenergic receptor agonist; (±)-epinephrine hydrochloride; Sigma-Aldrich). The adrenaline concentration was selected based on the results of Steele et al. (2011) showing that a reliable positive chronotropic effect was produced at 10^{-4} mol L^{-1} adrenaline. To evaluate breathing and heart rate responses, breathing frequency and heart rate were assessed for each 2 min interval during the 30 min exposure period, and the peak (maximum) response was identified.

2.5 Statistical analysis

Data are presented as mean values ± one standard error of the mean (SEM). Protein and mRNA abundances were compared between treatment groups using one-tailed Student's *t*-tests. Heart rate and ventilation frequency were evaluated by two-way repeated measures analysis of variance (RM ANOVA), with treatment group (sham or morphant) and exposure conditions (control, hypercapnia, and hypercapnia plus hypoxia or adrenaline) as the two factors. Where data did not meet the underlying assumptions of normality and equal variance, data were

transformed or two-way RM ANOVA was carried out on ranked data. A Holm-Sidak *post hoc* test was used for multiple comparisons when significant differences were detected by ANOVA. The fiducial limit of significance for all analyses was 0.05. Sigma-Plot (Version 11.1, SPSS Inc.) was used for all statistical analyses.

Table 2.1. Oligonucleotide primer pairs used for amplification of *kcnk5a* and *kcnk5b* by RT-PCR in zebrafish (*Danio rerio*) larvae and adult gill tissue.

Gene	T_a (°C)	Number of cycles	Product length (bp)	Primer sequence (5'to 3')
kcnk5a (exon-specific)	53	35	529	forward ATT GCA CTG TCG CG TTT ATG reverse GAA ACA CAG TGG CAC TCC AA
kcnk5a (intron-specific)	46.7	32	675	forward CGT AAG AGG AGA CTG ATT A reverse CCT ACA GAA GAC TCT AGC
kcnk5b	50	40	500	forward GGA GTG TGT GTT ACT TC reverse GAG CAA CTG ACT TAG AC
zatp6v1a	28	35	105	forward GAG GAA CCA CTG CCA TTC CA reverse CAA CCC ACA TAA ATG ATG ACA TCG

T_a, annealing temperature; *bp*, base pairs

Table 2.2. Oligonucleotide primer pairs used to generate a riboprobe against *kcnk5a*.

Riboprobe	Primer sequence (5'to 3')
kcnk5a anti-sense probe	forward-T7 GCG TAA TAC GAC TCA CTA TAG GAT TGC ACT GTC GCG TTT ATG reverse GAA ACA CAG TGG CAC TCC AA
kcnk5a sense probe	forward ATT GCA CTG TCG CG TTT ATG reverse-T7 GCG TAA TAC GAC TCA CTA TAG AAA CAC AGT GGC ACT CCA A

Table 2.3. Primary and secondary antibodies used for immunohistochemistry.

Antibody	Dilution	Antigen	Host	Source	Secondary antibody
Primary					
5-HT	1:100	serotonin	goat	ImmunoStar (ID: 20079)	Alexa 488 / Alexa 594
TASK-2	1:1000	*kcnk5a*[3]	rabbit	GenScript[1]	Alexa 488 / Alexa 568
TASK-2B	1:250	*kcnk5b*[4]	rabbit	GenScript[1]	Alexa 568
ZN-12	1:100	neuronal cell surface	mouse	DSHB[2]	Alexa 546 / CF™ 633
Secondary					
Alexa 488	1:250	goat	donkey	ThermoFisher Scientific (Cat #: A11055)	-----
Alexa 488	1:2000	rabbit	donkey	ThermoFisher Scientific (Cat #: A21206)	-----
Alexa 546	1:200	mouse	goat	ThermoFisher Scientific (Cat #:A11030 A)	-----
Alexa 568	1:2000	rabbit	donkey	ThermoFisher Scientific (Cat #: A10042)	-----
Alexa 594	1:250	goat	donkey	ThermoFisher Scientific (Cat #: A11058)	-----
CF™ 633	1:200	mouse	donkey	Sigma-Aldrich (Cat #: SAB4600131)	-----

[1]Custom antibody produced by GenScript (see text for details)

[2]Developmental Studies Hybridoma Bank, University of Iowa

[3] *kcnk5a* peptide sequence: CSDHGQSYERLVEEY

[4] *kcnk5b* peptide sequence: CVSEDRSLGKRSFG

Figure 2.1: Representative western blots for TASK-2 (A) and TASK-2b (B). In each panel, (a) represents protein from 4 dpf wild type zebrafish (*Danio rerio*) larvae probed with the primary antibody, (b) presents pre-immune serum probed with the primary antibody, and (c) is a pre-absorption control, where the primary antibody was pre-absorbed by incubating it with the peptide against which it was raised. The numbers indicate band sizes in kDa.

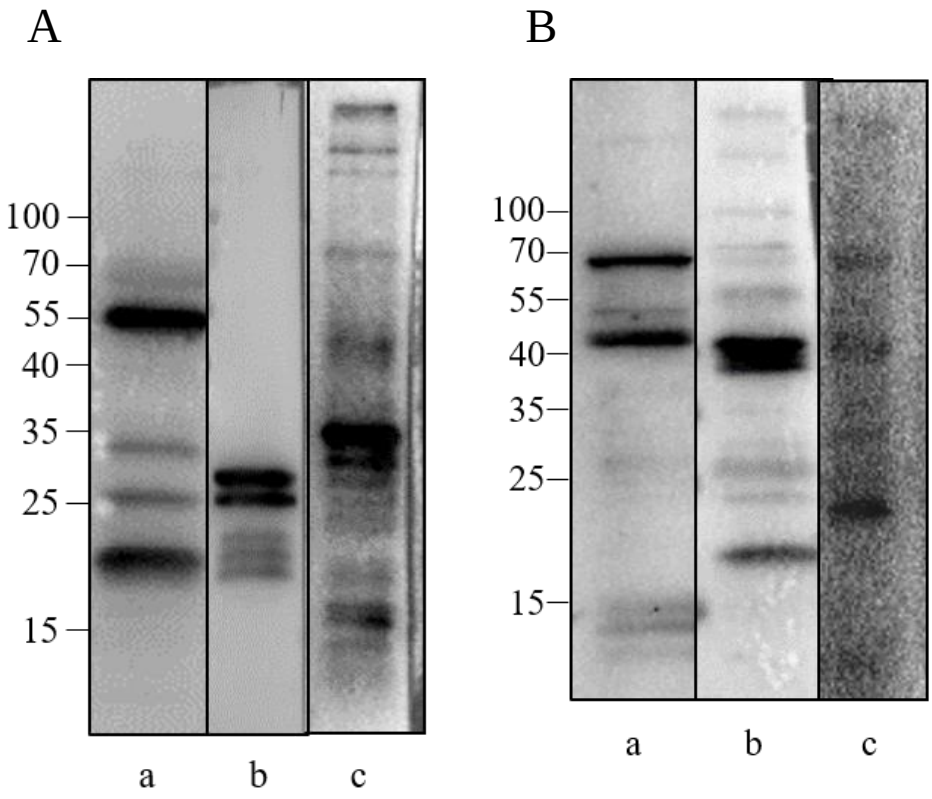
A
B
100
70
55
40
35
25
15
a
b
c
100
70
55
40
35
25
15
a
b
c

Figure 2.2: A schematic illustrating the expected effects of the binding to pre-mRNA of the splice-blocking antisense oligonucleotide morpholinos against *kcnk5a* (A) and *kcnk5b* (B). Lines represent intron sequences, gray rectangles represent exon sequences and white rectangles represent untranslated region (UTR) sequences. In panel A, the morpholino binds to a splice donor site (indicated by 1), preventing splicing out of the first intron, which is 15,199 bp long (2). In panel B, the morpholino binds to a splice acceptor site (1), causing the second exon (112 bp) to be spliced out (2).

A

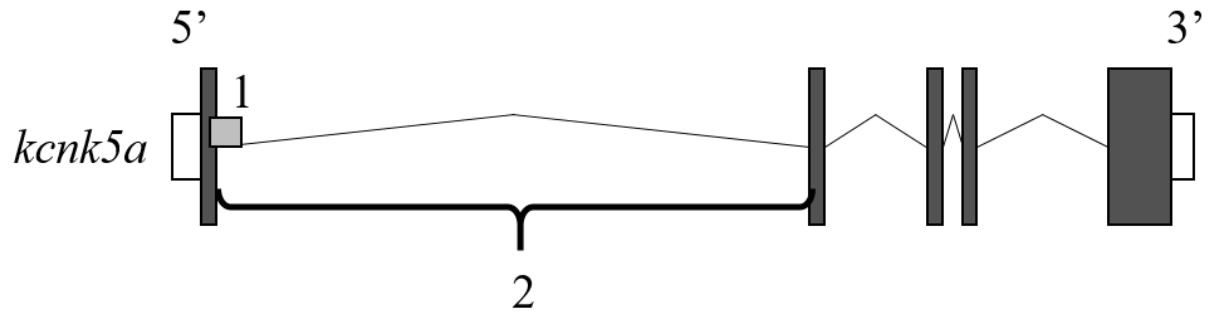

B

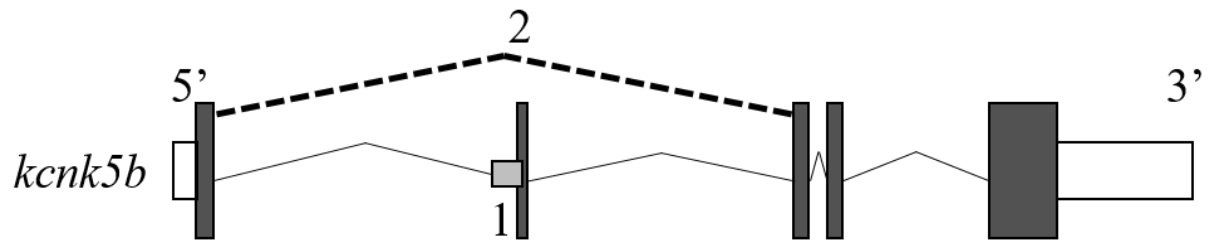

Figure 2.3: Representative western blots for TASK-2 and ß-actin (A), and TASK-2b and ß-actin (B), using a dilution series of protein samples, from 4 dpf wild-type zebrafish (*Danio rerio*) larvae, to identify the linear dynamic range for each antibody.

A

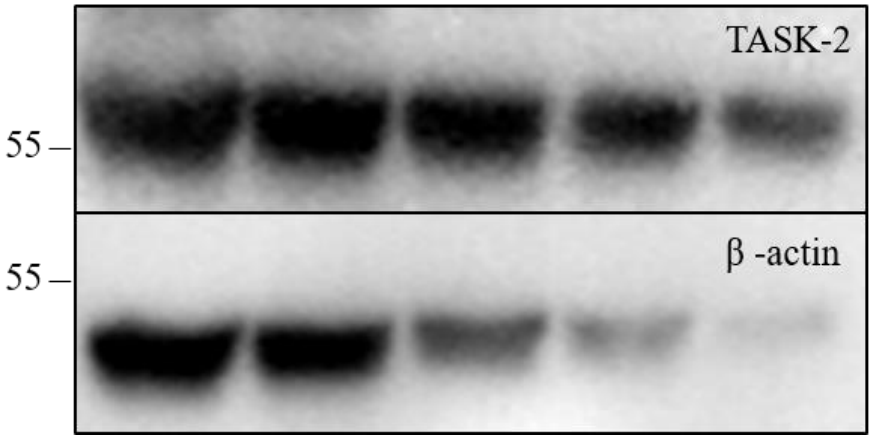
TASK-2
55
β -actin
55

B

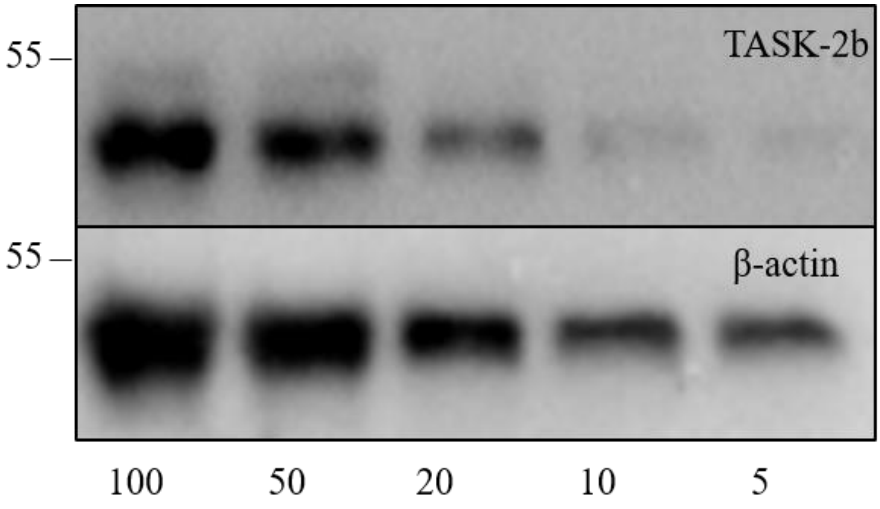
TASK-2b
55
β-actin
55
100
50
20
10
5
Protein loaded (µg)

Chapter 3: Results

3.1 Localization of *kcnk5*/TASK-2 paralogs in larval zebrafish and adult gill

After confirming by RT-PCR that *kcnk5a* and *kcnk5b* mRNA were present in 4 dpf zebrafish larvae (data not shown), the tissue distribution of *kcnk5a* mRNA was investigated using *in situ* hybridization. Owing to technical difficulties, *in situ* hybridization results were not obtained for *kcnk5b*. Imaging of 4 dpf zebrafish larvae revealed the presence of staining for *kcnk5a* mRNA in the brain and eye regions (Fig. 3.1A) as well as the epithelium surrounding the yolk sac, the swim bladder, and the dorsal side of the larvae (Fig. 3.1B). Staining was absent from negative control tissue sections that were incubated with a sense probe. Faint staining observed from negative control tissue sections can be attributed to over-staining (Fig. 3.1C-D).

Immunohistochemistry was used to investigate the tissue and cellular distribution of TASK-2 and TASK-2b, the protein products of *kcnk5a* and *kcnk5b*, respectively, both in whole larvae and in gill tissue from adult fish. Antibodies against 5-HT and the zebrafish neuronal marker zn-12 were used to identify NECs and nerves. In larvae, use of all three antibodies revealed what appeared to be TASK-2 labelling along nerves that innervated NECs; NECs were identified by virtue of 5-HT immunofluorescence (Fig. 3.2A, C-G). In addition, TASK-2 staining showed a faint ring-like pattern around the NEC (Fig. 3.2F). Unfortunately, no convincing immunofluorescence for TASK-2b was obtained in larval tissues even though the antibody against TASK-2b yielded satisfactory results in western blots. In adult gill tissue, co-labelling with 5-HT and TASK-2 revealed a stronger and clearer staining pattern on the surface of the NEC than that observed in larvae (Fig. 3.3). Again, a ring-like pattern of TASK-2 staining was observed around the NEC. But, in addition, there was also cytosolic staining (Fig. 3.3). Co-labelling with TASK-2 and zn-12 revealed that TASK-2 did not co-localize with nerve fibers

running along the gill filament and lamellae (Fig. 3.4). However, TASK-2-positive cells appeared to be innervated (Fig. 3.4). In adult gill tissue, TASK-2b did not co-localize with 5-HT (Fig. 3.5). Staining for TASK-2b was observed in small clusters of cells along the filament and the lamellae (Fig. 3.5B).

3.2 Knockdown of TASK-2 and TASK-2b

Antisense oligonucleotide morpholinos were used to knockdown TASK-2 and TASK-2b. To confirm that knockdown had been achieved, *kcnk5a* or *kcnk5b* mRNA expression was assessed by RT-PCR, and TASK-2 or TASK-2b protein expression was assessed by western blotting and/or immunohistochemistry. For the splice-blocking morpholino against *kcnk5a*, mRNA abundances were compared using primers that bound to regions in exons versus primers that bound to regions in the first intron, which was expected to be retained in the morphant larvae (Fig. 2.2). Whereas the exon-specific primers revealed a band of significantly diminished intensity in mRNA extracted from 4 dpf morphant larvae injected with the splice-blocking morpholino (Fig. 3.6A), the band obtained with intron-specific primers was significantly increased in intensity (Fig. 3.6B) relative to those observed for sham larvae injected with the control morpholino. In morphant larvae that had been injected with the *kcnk5a* translation blocking morpholino, TASK-2 protein levels were significantly decreased relative to those in sham larvae (Fig. 3.6C). Knockdown of TASK-2 also was confirmed by immunohistochemistry. In sham larvae that were injected with a control morpholino, a ring-like staining pattern was detected around NECs and this pattern was absent from morphant larvae that were injected with the *kcnk5a* splice–blocking morpholino (Fig. 3.7A-F), morphant larvae that were injected with

the *kcnk5a* translation–blocking morpholino (Fig. 3.7G-L), and double knockdown morphant larvae (i.e. those injected with both the *kcnk5a* translation-blocking and *kcnk5b* splice-blocking morpholinos) (Fig. 3.7M-R).

The splice-blocking morpholino against *kcnk5b* was expected to result in the loss of an exon, leading to a reduction in mRNA size (Fig. 2.2). Correspondingly, mRNA extracted from larvae injected with the control morpholino showed only a single band for *kcnk5b* whereas two bands were present in the *kcnk5b* morphant larvae (Fig. 3.8A), indicating successful knockdown. Western analysis for TASK-2b showed the absence of a band or a band that was greatly diminished in intensity despite equal protein loading (as indicated by ß-actin) in *kcnk5b* morphant larvae, confirming successful knockdown (Fig. 3.8B).

3.3 Cardiorespiratory response to hypercapnia in larval zebrafish

Sham larvae injected with the control morpholino responded to hypercapnia consistently throughout all trials with a significant increase in breathing and heart rates (Figs. 3.9-3.14). Addition of adrenaline (Figs. 3.9, 3.12) or exposure to hypoxia (Figs. 3.10, 3.11, 3.13, 3.14) while hypercapnia was maintained caused further increases in both ventilation and heart rate in sham larvae. The response to hypercapnia, but not that to adrenaline or hypoxia, was significantly blunted by knockdown of TASK-2 (Figs. 3.10-3.12), TASK-2b (Figs. 3.13-3.14), or both TASK-2 and TASK-2b together (Fig. 3.15). The morphant zebrafish larvae having a higher baseline reading did not prevent the larvae from further elevating ventilation frequency and heart rate.

Morphant larvae injected with the *kcnk5a* splice-blocking morpholino did not exhibit any significant differences in ventilation frequency or heart rate from the corresponding sham

group (Fig. 3.9A,B). However, the increases in breathing and heart rate between baseline and hypercapnic exposure conditions were significantly lower in *kcnk5a* MO larvae when compared with sham MO larvae (Fig. 3.9C,D). Addition of adrenaline had comparable effects on breathing and heart rates in sham and *kcnk5a* MO larvae (Fig. 3.9C,D). Interestingly, in a separate trial carried out using the *kcnk5a* splice-blocking morpholino and hypoxia rather than adrenaline, heart rate in *kcnk5a* MO larvae was significantly higher than that in sham larvae, while breathing rate was significantly higher in *kcnk5a* MO larvae under baseline conditions (Fig. 3.10A,B). Again, the increases in breathing and heart rates between baseline and hypercapnic exposure conditions were significantly reduced in *kcnk5a* MO larvae when compared with sham larvae (Fig. 3.10C,D). Also, during hypercapnia, *kcnk5a* MO larvae exhibited a significantly greater heart rate response to hypoxia when compared with the sham group. Similar patterns were observed for morphant larvae that were injected with the *kcnk5a* translation-blocking morpholino (Fig. 3.11). In this trial, *kcnk5a* MO larvae exhibited significantly higher ventilation and heart rates than sham larvae (Fig. 3.11A,B) and the increases in breathing and heart rates during hypercapnia were significantly lower in *kcnk5a* MO larvae (Fig. 3.11C,D). No differences in the response to hypoxia were observed between sham and *kcnk5a* MO larvae (Fig. 3.11C,D)

For morphant larvae injected with the *kcnk5b* splice-blocking morpholino, baseline heart rate and breathing frequency were significantly higher than in sham larvae in trials using adrenaline (Fig. 3.12A,B). The increases in heart and breathing rates during hypercapnia were significantly blunted in the *kcnk5b* morphants, although no differences were observed in the responses to adrenaline (Fig. 3.12C,D). Similarly, in a separate trial, the increases in heart and breathing rates during hypercapnic exposure were significantly higher in sham larvae than in *kcnk5b* morphants, with no difference in the response to hypoxia (Fig. 3.13C,D). In this case,

however, baseline breathing frequency and heart rate, as well as heart rate in response to hypoxia were significantly higher in *kcnk5b* morphant larvae than sham larvae (Fig. 3.13A,B).

In morphant larvae injected with combined *kcnk5a* and *kcnk5b* morpholinos, a blunted response was observed in response to hypercapnia for both breathing frequency and heart rate (Fig. 3.14C,D). Breathing and heart rates were increased by additional exposure to hypoxia (with hypercapnia), and the breathing frequency response in *kcnk5a +5b* morphant larvae was significantly greater than that in sham larvae (Fig. 3.14C,D). Double morphant larvae exhibited significantly higher baseline breathing and heart rates when compared with sham larvae (Fig. 3.14A,B).

Figure 3.1: Representative light micrographs reveal by *in situ* hybridization the presence of *kcnk5a* mRNA in 4 dpf wild type zebrafish (*Danio rerio*) larvae. Using an antisense riboprobe, colouration associated with the presence of *kcnk5a* mRNA was detected in both the head (A) and yolk sac (B). Colour development did not occur in corresponding tissue sections incubated with a sense probe (C, D). Red lines in panel E indicate the approximate locations of the sections. Black arrow heads indicate staining for *kcnk5a* mRNA. Scale bar = 100 µm

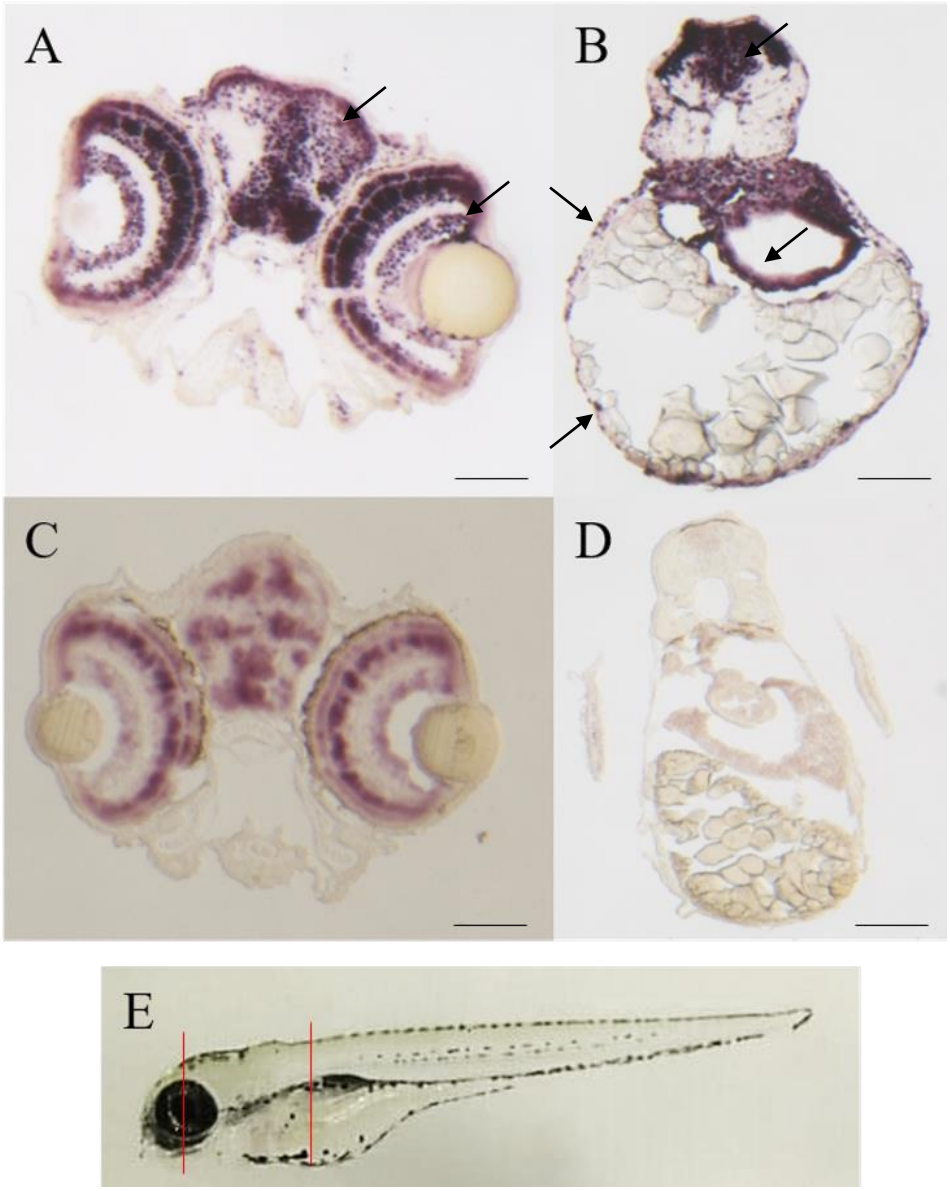
A
B
C
D
E

Figure 3.2: Representative light micrographs reveal by immunohistochemistry the presence of TASK-2 (in red), 5-HT (in green) and nerves (in white), using the zn-12 antibody, in the tail region of a 4 dpf zebrafish (*Danio rerio*) larva. Panel A is a low magnification image of multiple NECs with staining for 5-HT. Panel C presents an overlay of staining for TASK-2, 5-HT and zn-12, and panel D is a higher magnification image of the neuroepithelial cell (NEC) outlined by the white box in C. Immunofluorescence associated with 5-HT, TASK-2 and zn-12 is shown individually for this NEC in panels E to G, respectively, while panel B indicates the region of the tail that was imaged. Co-localization of TASK-2 and 5-HT is apparent in the NEC. Scale bar = 10 µm.

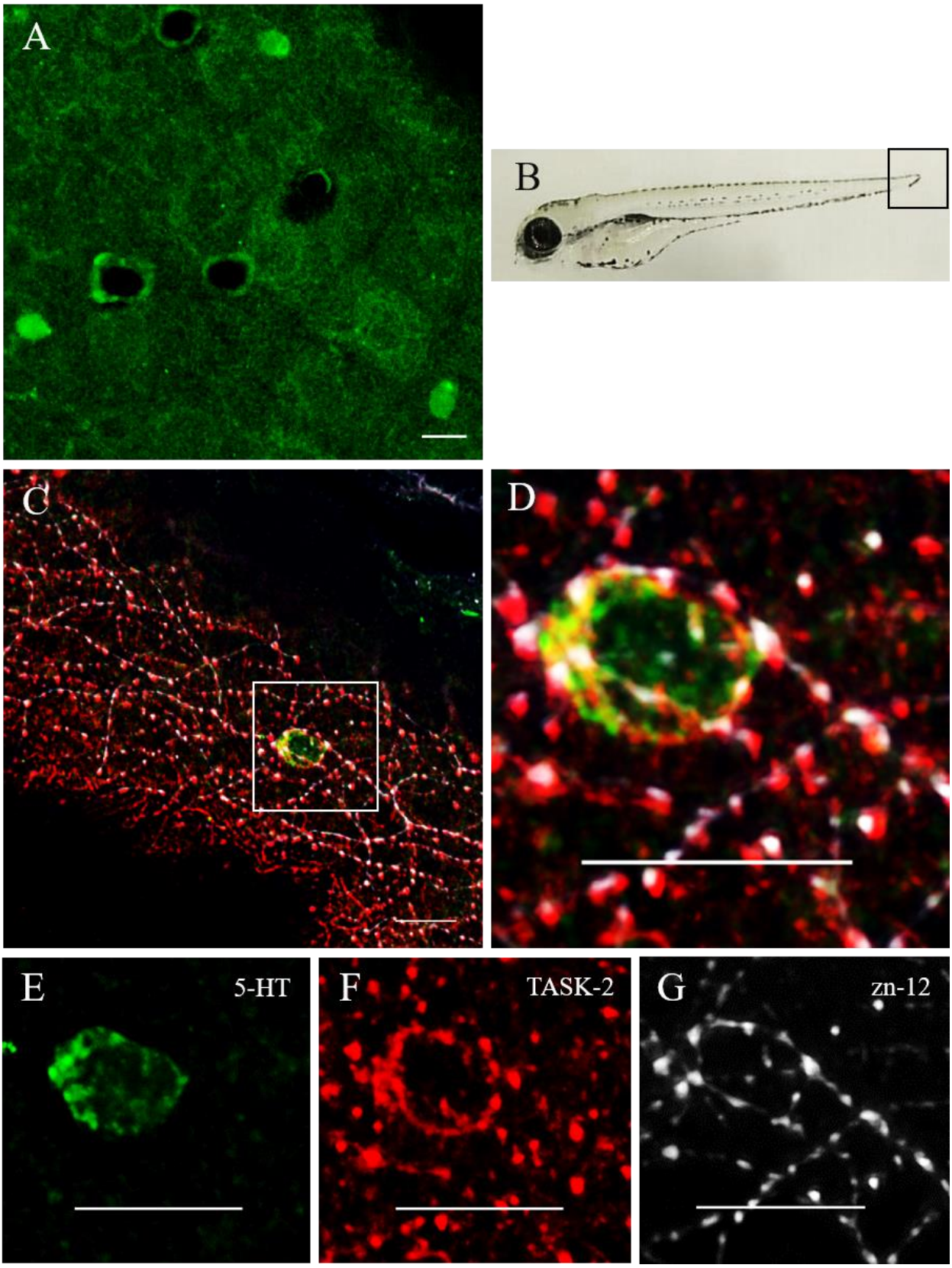
A
B
C
D
E
5-HT
F
TASK-2
G
zn-12

Figure 3.3: Representative light micrographs reveal by immunohistochemistry the presence of TASK-2 (in green) and 5-HT (in red) in neuroepithelial cells (NEC) of the gill filament of an adult zebrafish (*Danio rerio*). Panel A presents an overlay of staining for TASK-2 and 5-HT, and panel B is a higher magnification image of the NEC outlined by the white box in A. Immunofluorescence associated with 5-HT and TASK-2 is shown individually for this NEC in panels C and D, respectively, while panel E is a schematic indicating the region of the gill that was imaged. Co-localization of TASK-2 and 5-HT is apparent in NECs. Scale bar = 50 μm (A) and 10 μm (B-D).

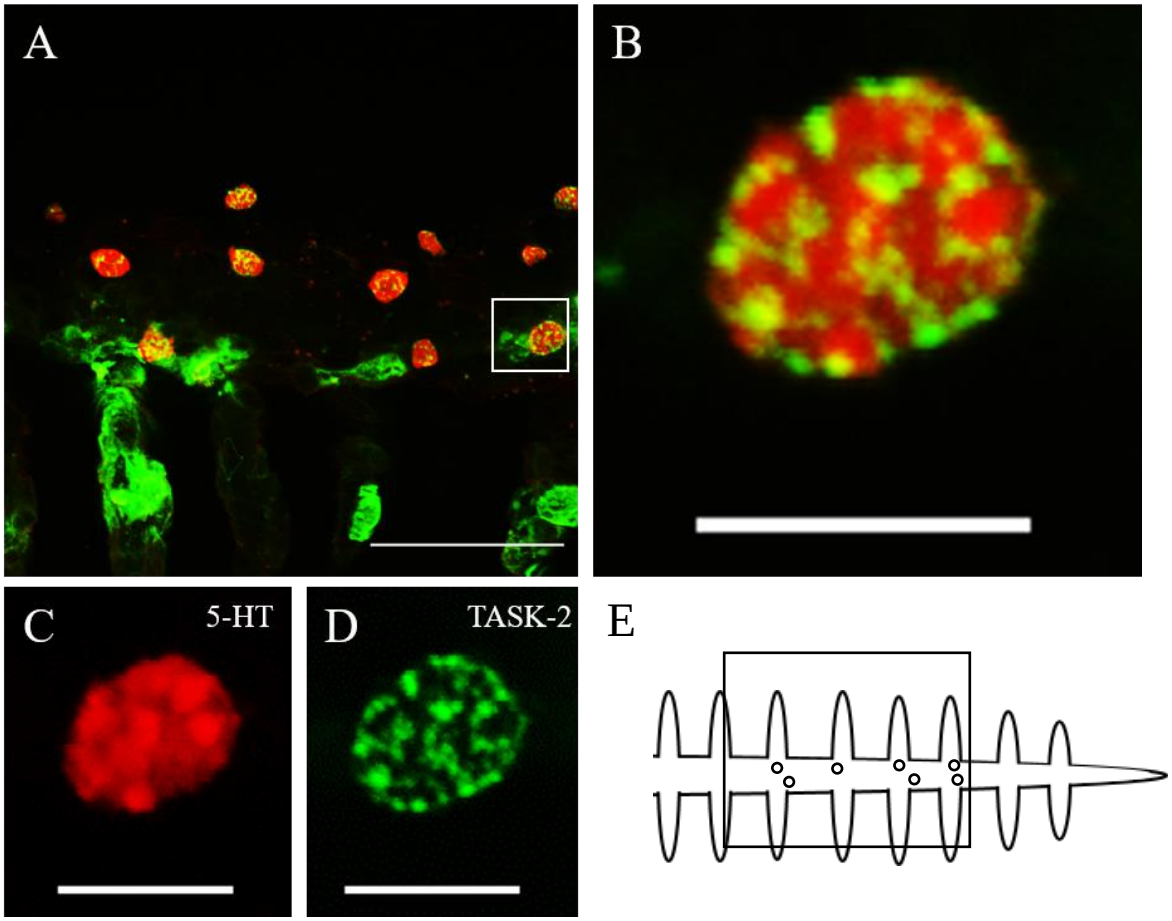
A
B
C
5-HT
D
TASK-2
E

Figure 3.4: Representative light micrographs reveal by immunohistochemistry the presence of TASK-2 (in green) and nerves (in red), using the zn-12 antibody, in the gill filament of an adult zebrafish (*Danio rerio*). Panel A presents immunofluorescence associated with zn-12, panel B shows immunofluorescence associated with TASK-2, and panel C is an overlay of A and B. Panel D is a schematic indicating the region of the gill that was imaged. No co-localization of TASK-2 and zn-12 was apparent, although zn-12-labelled nerve fibres appeared to innervate TASK-2-positive cells (white arrow heads in panel C). Scale bar = 100 μm.

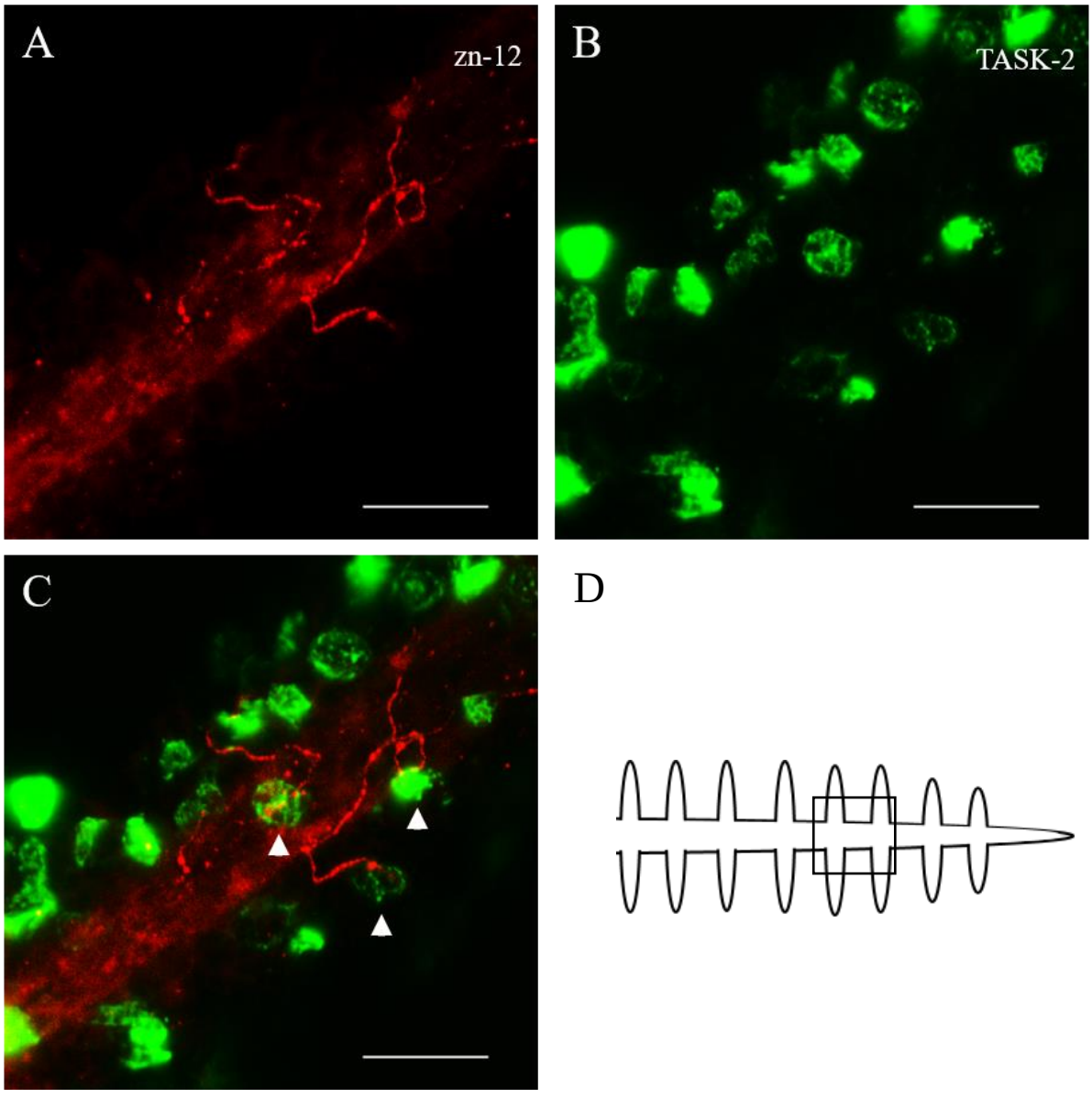
A
zn-12
B
TASK-2
C
D

Figure 3.5: Representative light micrographs reveal by immunohistochemistry the presence of TASK-2b (in red) and 5-HT (in green) in the gill filament of an adult zebrafish (*Danio rerio*). Panel A presents immunofluorescence associated with 5-HT, panel B shows immunofluorescence associated with TASK-2b, and panel C is an overlay of A and B. Panel D is a schematic indicating the region of the gill that was imaged. No co-localization of TASK-2b and 5-HT was detected in the gill filament. Scale bar = 50 µm.

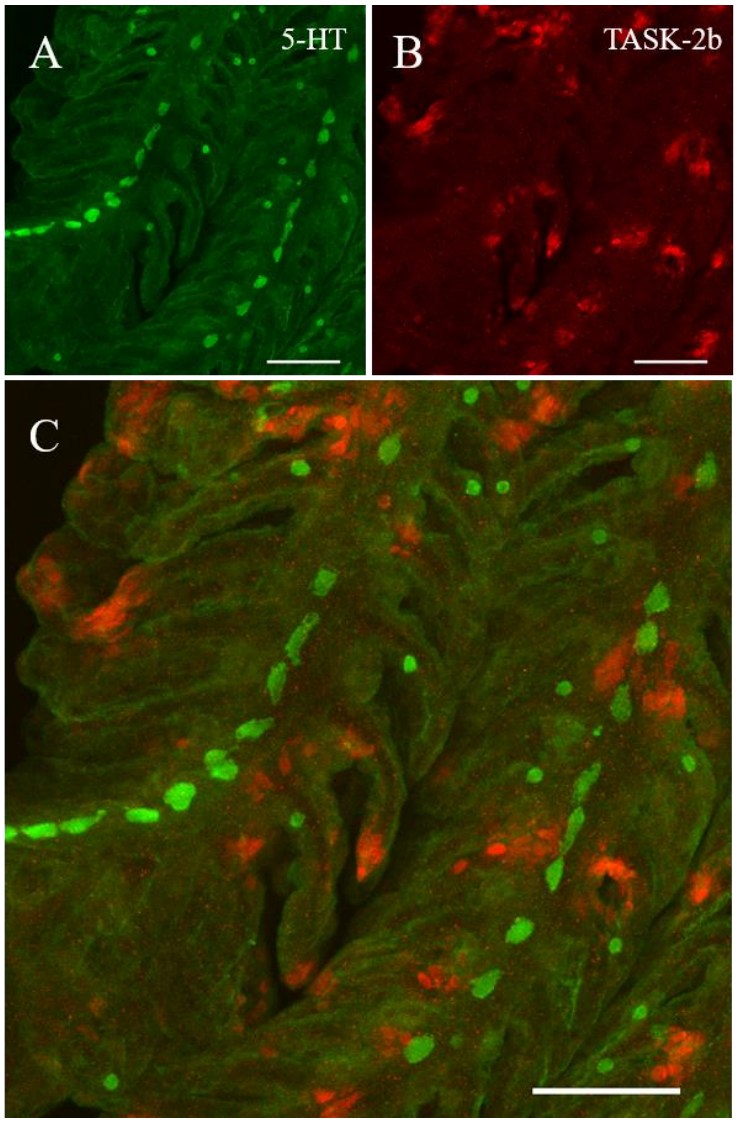

D

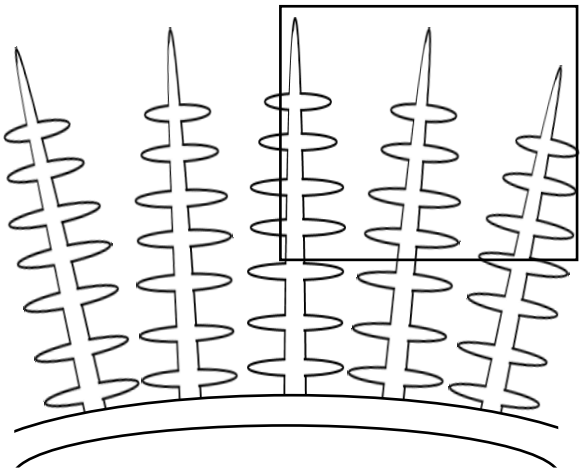

Figure 3.6: Confirmation of knockdown for the *kcnk5a* splice-blocking morpholino by RT-PCR (A, B) and for the *kcnk5a* translation-blocking morpholino by western analysis (C). Whereas the expression of *kcnk5a* detected using exon-specific primers was significantly reduced in morphant (MO) relative to sham larvae (A), the expression of *kcnk5a* detected using intron-specific primers was significantly higher in morphants (B). The inset images present representative gels of PCR products. Expression of V-type H^+-ATPase (*zatp6v1a*) was used as a control. In (C), the abundance of TASK-2 protein was significantly reduced in morphant relative to sham larvae, with the inset image presenting representative western blots. Values are means ± SEM with N = 4 in panel A, 5 in panel B and 6 in panel C. An asterisk indicates a significant difference between sham and morphant larvae (Student's *t*-test, $P = 0.03$ in panel A, 0.012 in panel B and one-tailed Student's *t*-test, $P = 0.037$ in panel C).

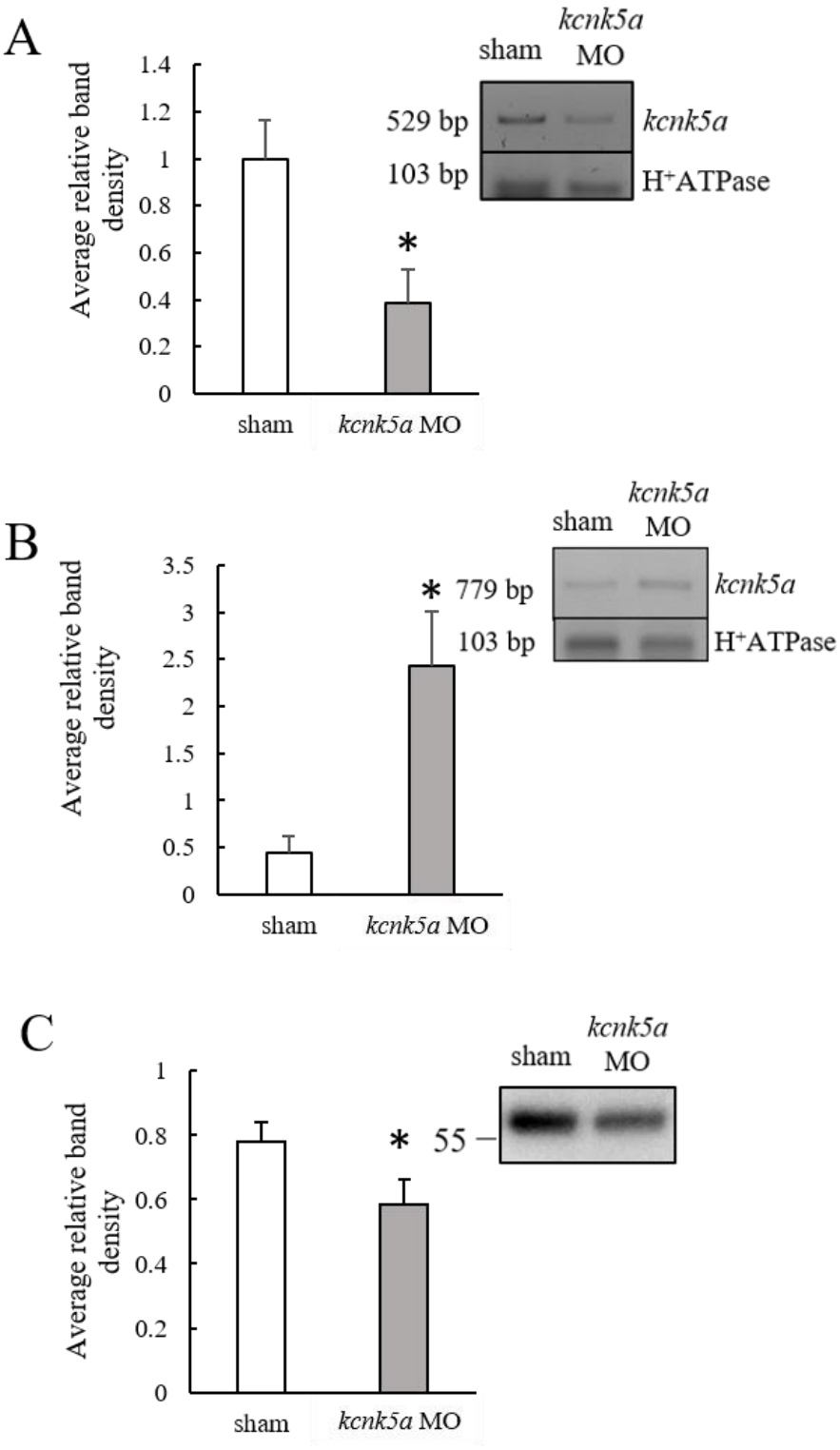
A
kcnk5a
sham
MO
529 bp
kcnk5a
103 bp
H+ATPase
Average relative band density
1.4
1.2
1
0.8
0.6
0.4
0.2
0
*
sham
kcnk5a MO
B
kcnk5a
sham
MO
* 779 bp
kcnk5a
103 bp
H+ATPase
Average relative band density
3.5
3
2.5
2
1.5
1
0.5
0
sham
kcnk5a MO
C
kcnk5a
sham
MO
* 55 –
Average relative band density
1
0.8
0.6
0.4
0.2
0
sham
kcnk5a MO

Figure 3.7: Representative light micrographs of skin neuroepithelial cells (NECs) from sham (A-C, G-I, and M-O) and morpholino-injected 4 dpf zebrafish (*Danio rerio*) larvae (D-F, J-L, and P-R). These images were drawn from the 3-4 larvae that were examined in each treatment. Images for larvae injected with the *kcnk5a* splice-blocking morpholino are presented in panels E-G, the *kcnk5a* translation-blocking morpholino in panels K-M, and the *kcnk5a* translation-blocking together with the *kcnk5b* splice-blocking morpholino (i.e. double knockdown) in panels P-R. Each set of images presents immunofluorescence associated with 5-HT (in green) in the first image, TASK-2 (in red) in the second image, and an overlay of 5-HT and TASK-2 in the third image. In each pair of sham/morphant images, immunofluorescence associated with TASK-2 can be observed as a ring around the NEC in the sham but not the morphant larvae. Scale bar = 10 μm.

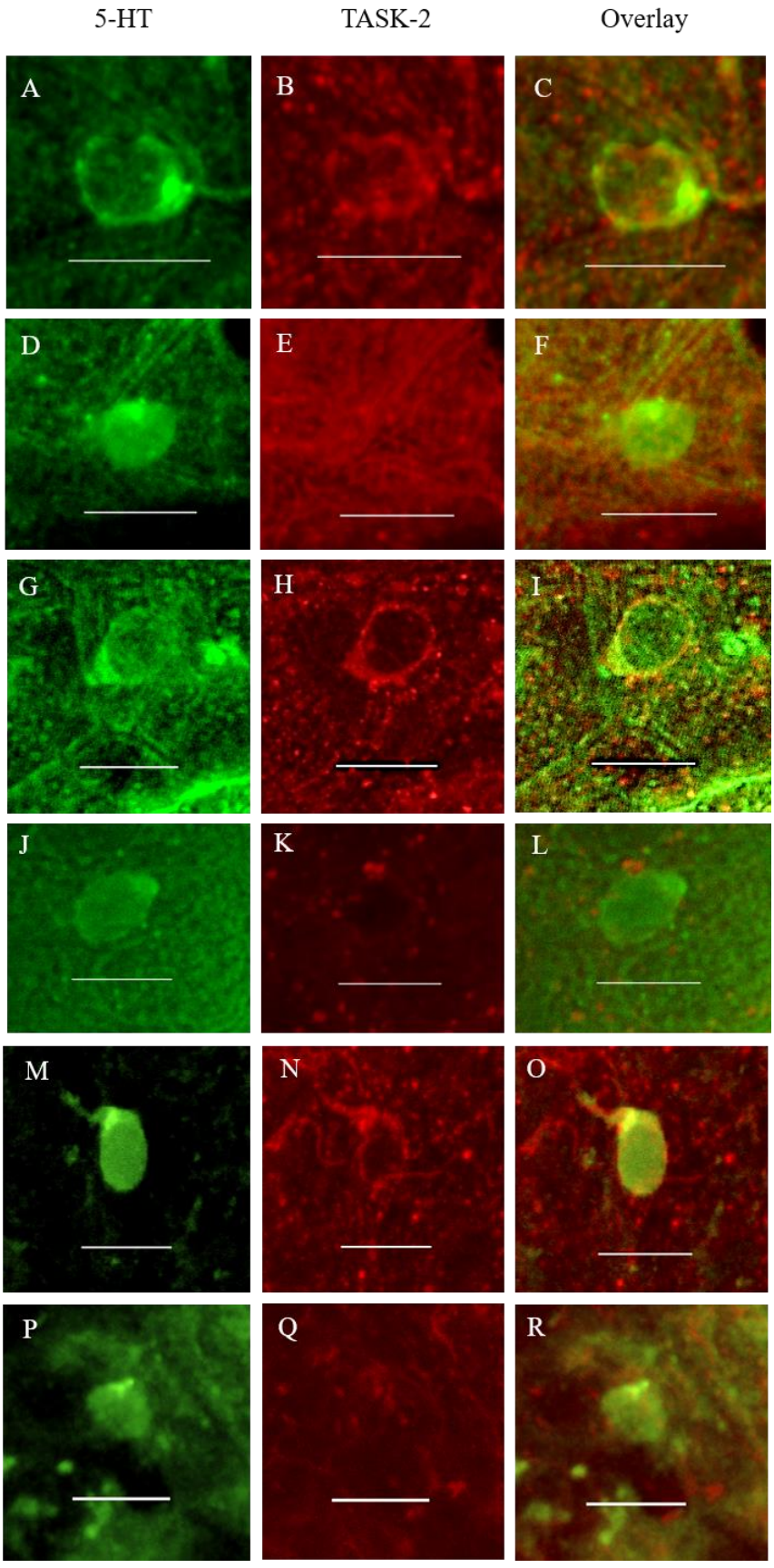
5-HT
TASK-2
Overlay
A
B
C
D
E
F
G
H
I
J
K
L
M
N
O
P
Q
R

Figure 3.8: Representative images demonstrating confirmation of knockdown for the *kcnk5b* splice-blocking morpholino by RT-PCR (A) and western analysis (B) for four individual pairs of sham and morphant larvae. In panel A, a second band of smaller size is detected using primers against *kcnk5b* in morphant but not sham larvae (band sizes indicated on the left side of the image in bp). In panel B, morphant larvae did not express TASK-2b protein (at 50.3 kDa; band sizes indicated on the left side of the image in kDa) or showed greatly reduced levels of TASK-2b protein relative to sham larvae, despite similar abundances of ß-actin.

A

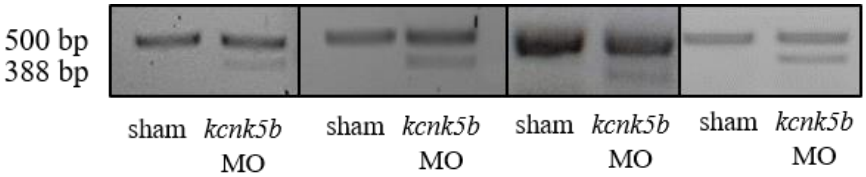
500 bp
388 bp
sham
kcnk5b MO
sham
kcnk5b MO
sham
kcnk5b MO
sham
kcnk5b MO

B

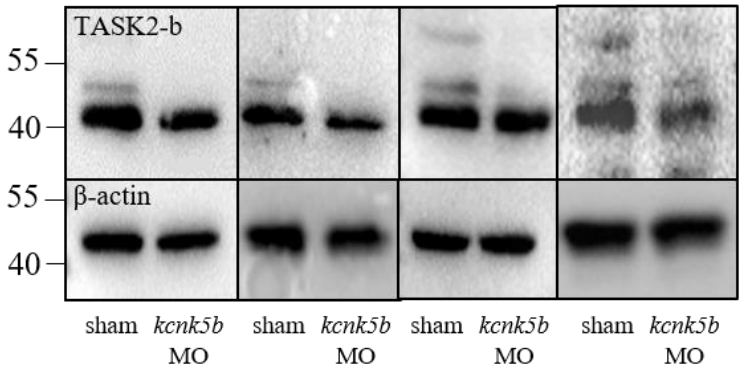
TASK2-b
55
40
β-actin
55
40
sham
kcnk5b MO
sham
kcnk5b MO
sham
kcnk5b MO
sham
kcnk5b MO

Figure 3.9: The effect of *kcnk5a* knockdown (using the splice-blocking morpholino) on ventilation frequency (f_R; A) and heart rate (f_H; B) in 4 dpf zebrafish (*Danio rerio*) larvae exposed to normoxic normocapnia (baseline), hypercapnia (1.5% CO_2), or 10^{-4} mol L^{-1} adrenaline under hypercapnic conditions. In panel A, only the main effect of exposure condition was significant (two-way RM ANOVA on ranks, $P < 0.001$) and pairs of bars that share a letter are not significantly different from one another. In panel B, a significant interaction between exposure condition and treatment group was detected (two-way RM ANOVA, $P < 0.001$) and bars that share a letter are not significantly different from one another. The effect of *kcnk5a* knockdown on changes in ventilation frequency (C) and heart rate (D) between exposure conditions also is presented. An asterisk indicates a significant difference between sham and *kcnk5a* morphant larvae (for C, rank sum test, $P = 0.019$ and Student's *t*-test, $P = 0.647$; for D, Student's *t*-test, $P < 0.001$ and 0.858). Values are means + SEM, $N = 10$.

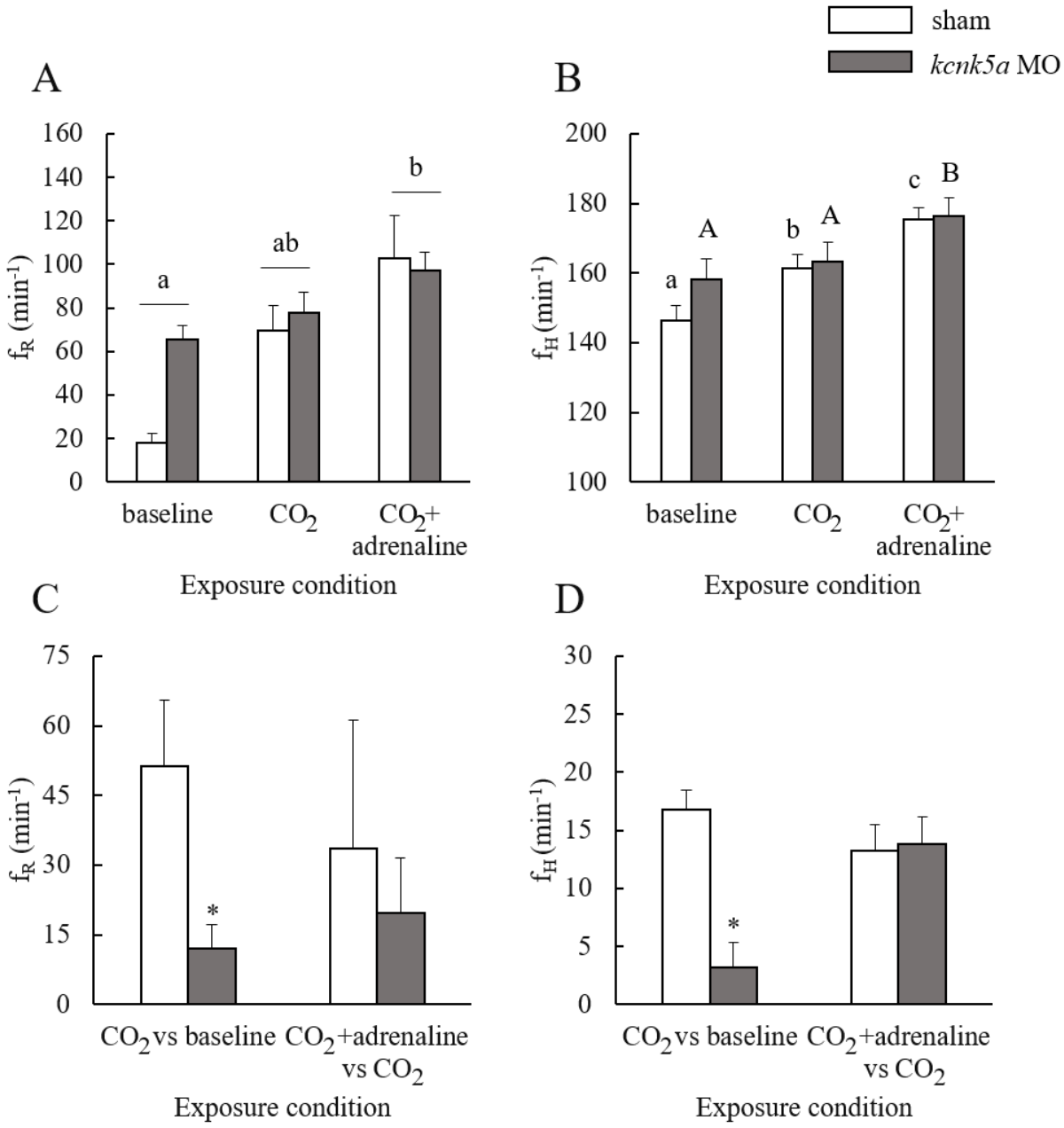
sham
kcnk5a MO
A
B
C
D
f_R (min^{-1})
f_H (min^{-1})
a
ab
b
A
B
c
*
baseline
CO_2
CO_2+ adrenaline
CO_2vs baseline
CO_2+adrenaline vs CO_2
Exposure condition

Figure 3.10: The effect of *kcnk5a* knockdown (using the splice-blocking morpholino) on ventilation frequency (f_R; A) and heart rate (f_H; B) in 4 dpf zebrafish (*Danio rerio*) larvae exposed to normoxic normocapnia (baseline), hypercapnia (1.5% CO_2), or hypoxic (water O_2 tension of 30 mmHg) hypercapnia (1.5% CO_2). In panel A, a significant interaction between exposure condition and treatment group was detected (two-way RM ANOVA, $P = 0.036$); bars that share a letter are not significantly different from one another and an asterisk indicates a significant difference between sham and morphant larvae. In panel B, both main effects were significant (two-way RM ANOVA, $P < 0.001$ in each case), but the interaction between exposure condition and treatment group was not. Pairs of bars that share a letter are not significantly different from one another. The effect of *kcnk5a* knockdown on changes in ventilation frequency (C) and heart rate (D) between exposure conditions also is presented. An asterisk indicates a significant difference between sham and *kcnk5a* morphant larvae (for C, Student's *t*-test, $P = 0.0413$ and 0.791; for D, one-tailed Student's *t*-test, $P < 0.0339$ and 0.0495). Values are means + SEM, $N = 5$.

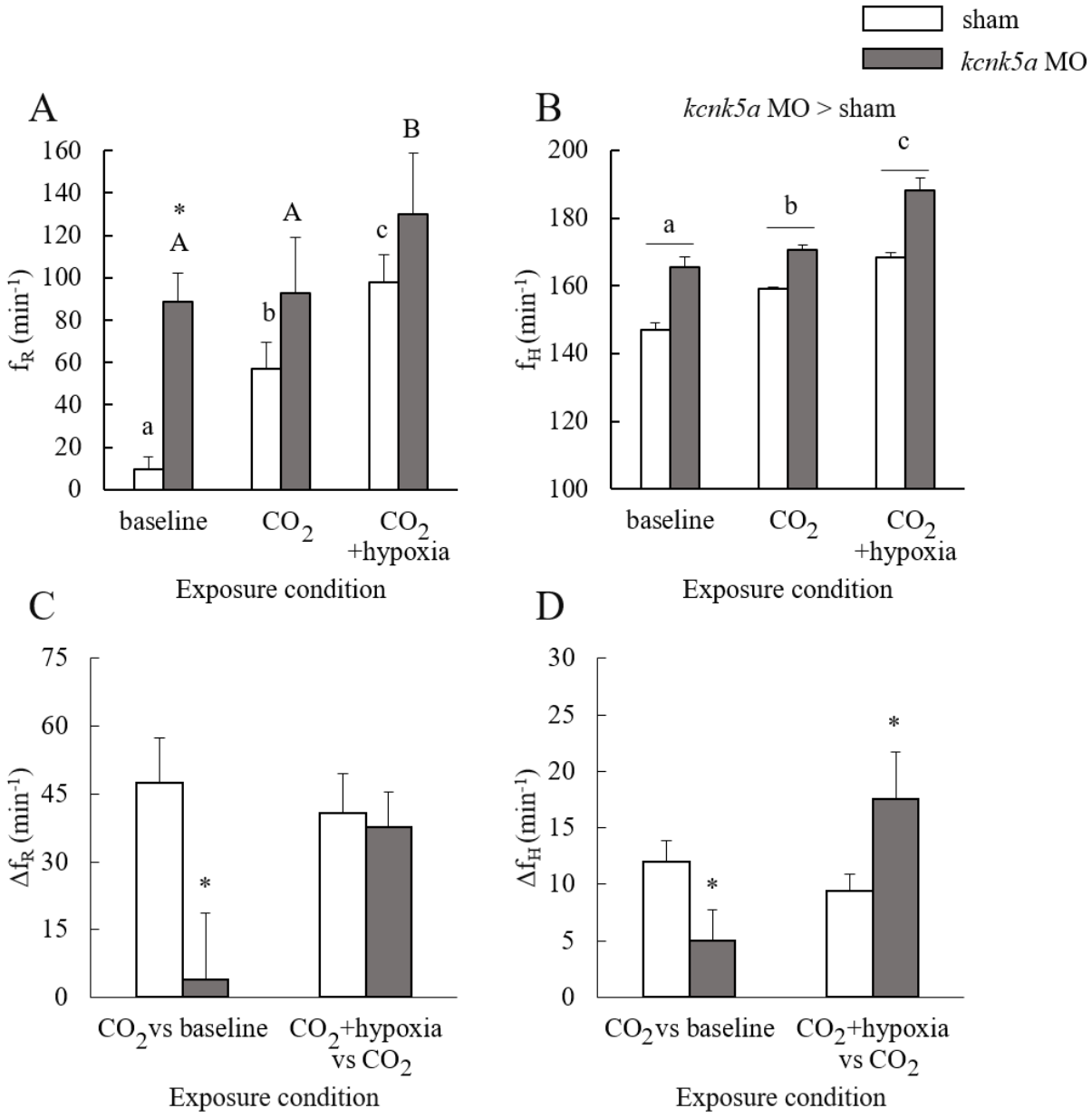
sham
kcnk5a MO
A
B
kcnk5a MO > sham
C
D
baseline
CO2
CO2 +hypoxia
Exposure condition
fR (min-1)
fH (min-1)
ΔfR (min-1)
ΔfH (min-1)
CO2vs baseline
CO2+hypoxia vs CO2

Figure 3.11: The effect of *kcnk5a* knockdown (using the translation-blocking morpholino) on ventilation frequency (f_R; A) and heart rate (f_H; B) in 4 dpf zebrafish (*Danio rerio*) larvae exposed to normoxic normocapnia (baseline), hypercapnia (1.5% CO_2), or hypoxic (water O_2 tension of 30 mmHg) hypercapnia (1.5% CO_2). In panel A, both main effects were significant (two-way RM ANOVA, $P < 0.001$ in each case), but the interaction between exposure condition and treatment group was not. Pairs of bars that share a letter are not significantly different from one another. In panel B, a significant interaction between exposure condition and treatment group was detected (two-way RM ANOVA, $P = 0.003$); bars that share a letter are not significantly different from one another and an asterisk indicates a significant difference between sham and morphant larvae. The effect of *kcnk5a* knockdown on changes in ventilation frequency (C) and heart rate (D) between exposure conditions also is presented. An asterisk indicates a significant difference between sham and *kcnk5a* morphant larvae (for C, Student's *t*-test, $P = 0.001$ and 0.595; for D, Student's *t*-test, $P < 0.00496$ and rank sum test, $P = 0.531$). Values are means + SEM, $N = 9$.

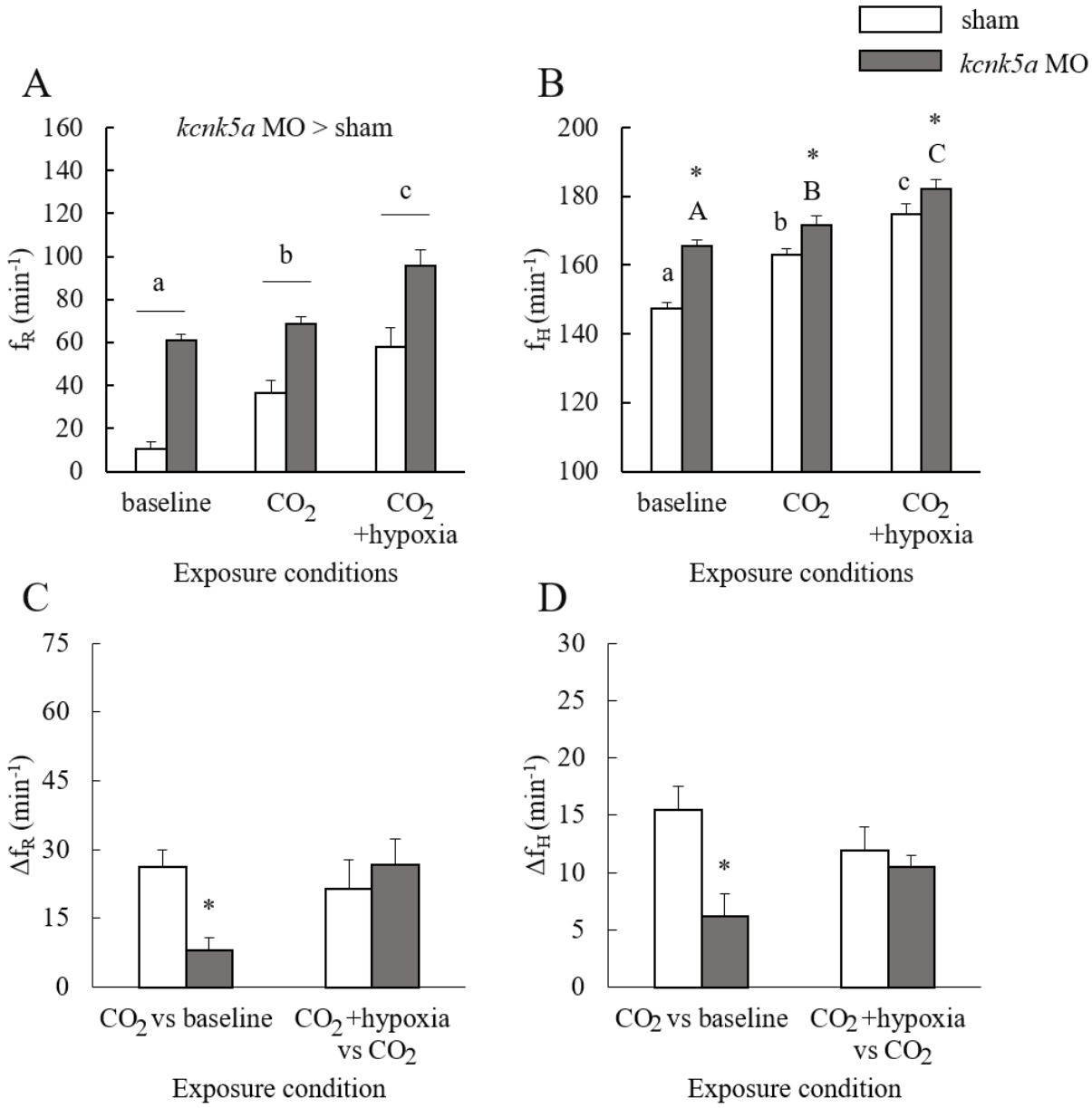
sham
kcnk5a MO
A
kcnk5a MO > sham
160
140
120
100
80
60
40
20
0
f_R (min^-1)
a
b
c
baseline
CO2
CO2 +hypoxia
Exposure conditions
B
200
180
160
140
120
100
f_H (min^-1)
a
b
c
A
B
C
*
baseline
CO2
CO2 +hypoxia
Exposure conditions
C
75
60
45
30
15
0
Δf_R (min^-1)
*
CO2 vs baseline
CO2 +hypoxia vs CO2
Exposure condition
D
30
25
20
15
10
5
0
Δf_H (min^-1)
*
CO2 vs baseline
CO2 +hypoxia vs CO2
Exposure condition

Figure 3.12: The effect of *kcnk5b* knockdown (using the splice-blocking morpholino) on ventilation frequency (f_R; A) and heart rate (f_H; B) in 4 dpf zebrafish (*Danio rerio*) larvae exposed to normoxic normocapnia (baseline), hypercapnia (1.5% CO_2), or 10^{-4} mol L^{-1} adrenaline under hypercapnic conditions. In panel A, a significant interaction between exposure condition and treatment group was detected (two-way RM ANOVA on log-transformed data, P = 0.002); bars that share a letter are not significantly different from one another and an asterisk indicates a significant difference between sham and morphant larvae. In panel B, both main effects were significant (two-way RM ANOVA, $P < 0.001$ in each case), but the interaction between exposure condition and treatment group was not. Pairs of bars that share a letter are not significantly different from one another. The effect of *kcnk5b* knockdown on changes in ventilation frequency (C) and heart rate (D) between exposure conditions also is presented. An asterisk indicates a significant difference between sham and *kcnk5b* morphant larvae (for C, Student's *t*-test, P = 0.000341 and 0.889; for D, rank sum test, P = 0.029 and Student's *t*-test, P = 0.441). Values are means + SEM, N = 7 for sham and 8 for *kcnk5b* morphant larvae.

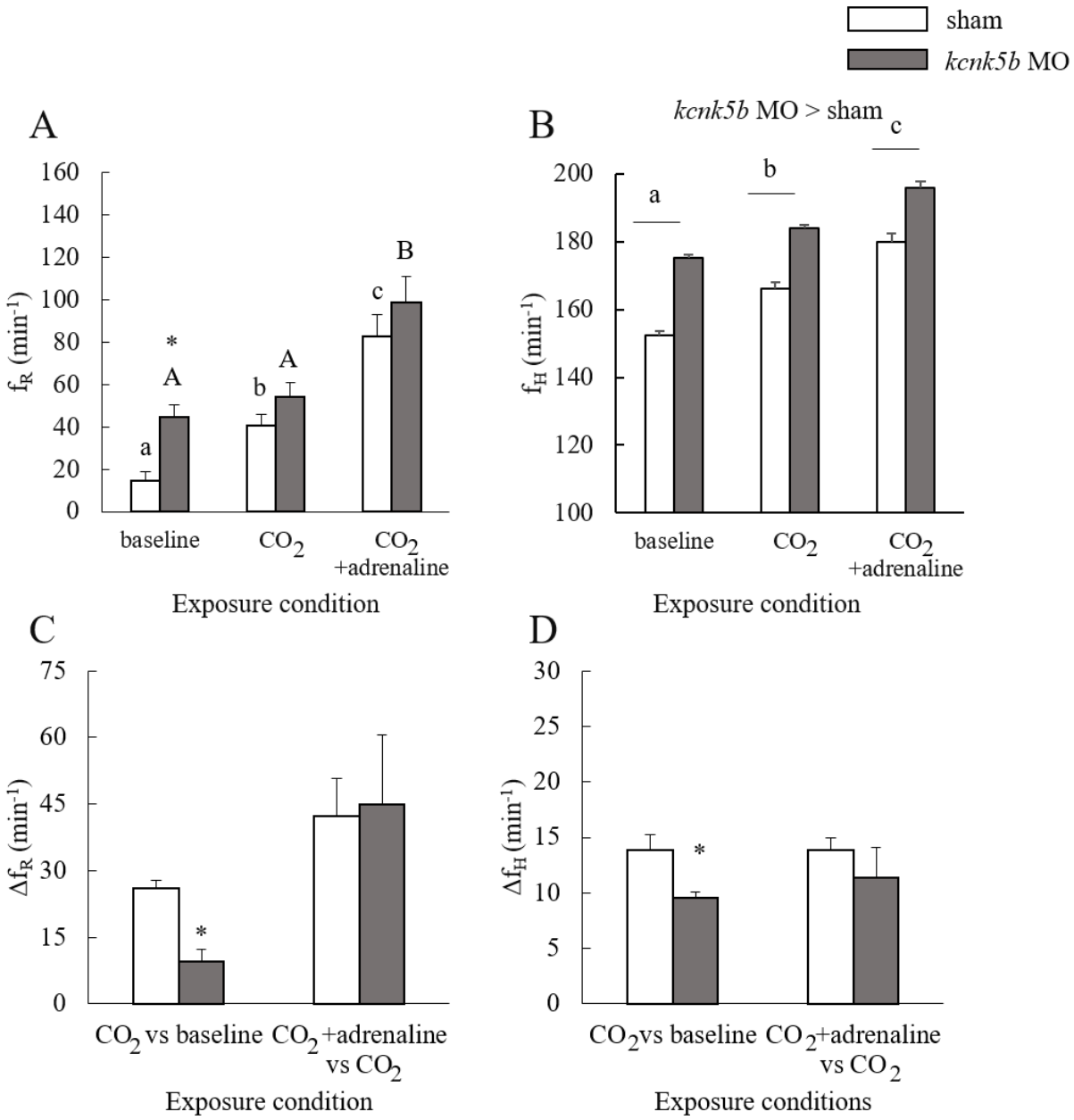
sham
kcnk5b MO
A
160
140
120
100
80
60
40
20
0
f_R (min^{-1})
a
A
b
A
c
B
*
baseline
CO_2
CO_2 +adrenaline
Exposure condition
B
kcnk5b MO > sham
200
180
160
140
120
100
f_H (min^{-1})
a
b
c
baseline
CO_2
CO_2 +adrenaline
Exposure condition
C
75
60
45
30
15
0
Δf_R (min^{-1})
*
CO_2 vs baseline
CO_2 +adrenaline vs CO_2
Exposure condition
D
30
25
20
15
10
5
0
Δf_H (min^{-1})
*
CO_2 vs baseline
CO_2 +adrenaline vs CO_2
Exposure conditions

Figure 3.13: The effect of *kcnk5b* knockdown (using a splice-blocking morpholino) on ventilation frequency (f_R; A) and heart rate (f_H; B) in 4 dpf zebrafish (*Danio rerio*) larvae exposed to normoxic normocapnia (baseline), hypercapnia (1.5% CO_2), or hypoxic (water O_2 tension of 30 mmHg) hypercapnia (1.5% CO_2). In panel A, a significant interaction between exposure condition and treatment group was detected (two-way RM ANOVA, $P < 0.001$); bars that share a letter are not significantly different from one another and an asterisk indicates a significant difference between sham and morphant larvae. In panel B, a significant interaction between exposure condition and treatment group was detected (two-way RM ANOVA, $P < 0.001$); bars that share a letter are not significantly different from one another and an asterisk indicates a significant difference between sham and morphant larvae. The effect of *kcnk5b* knockdown on changes in ventilation frequency (C) and heart rate (D) between exposure conditions also is presented. An asterisk indicates a significant difference between sham and *kcnk5b* morphant larvae (for C, rank sum test, $P < 0.001$ and Student's *t*-test, $P = 0.627$; for D, rank sum test, $P < 0.001$ and Student's *t*-test, $P = 0.166$). Values are means + SEM, $N = 7$ for sham and 8 for morphant larvae.

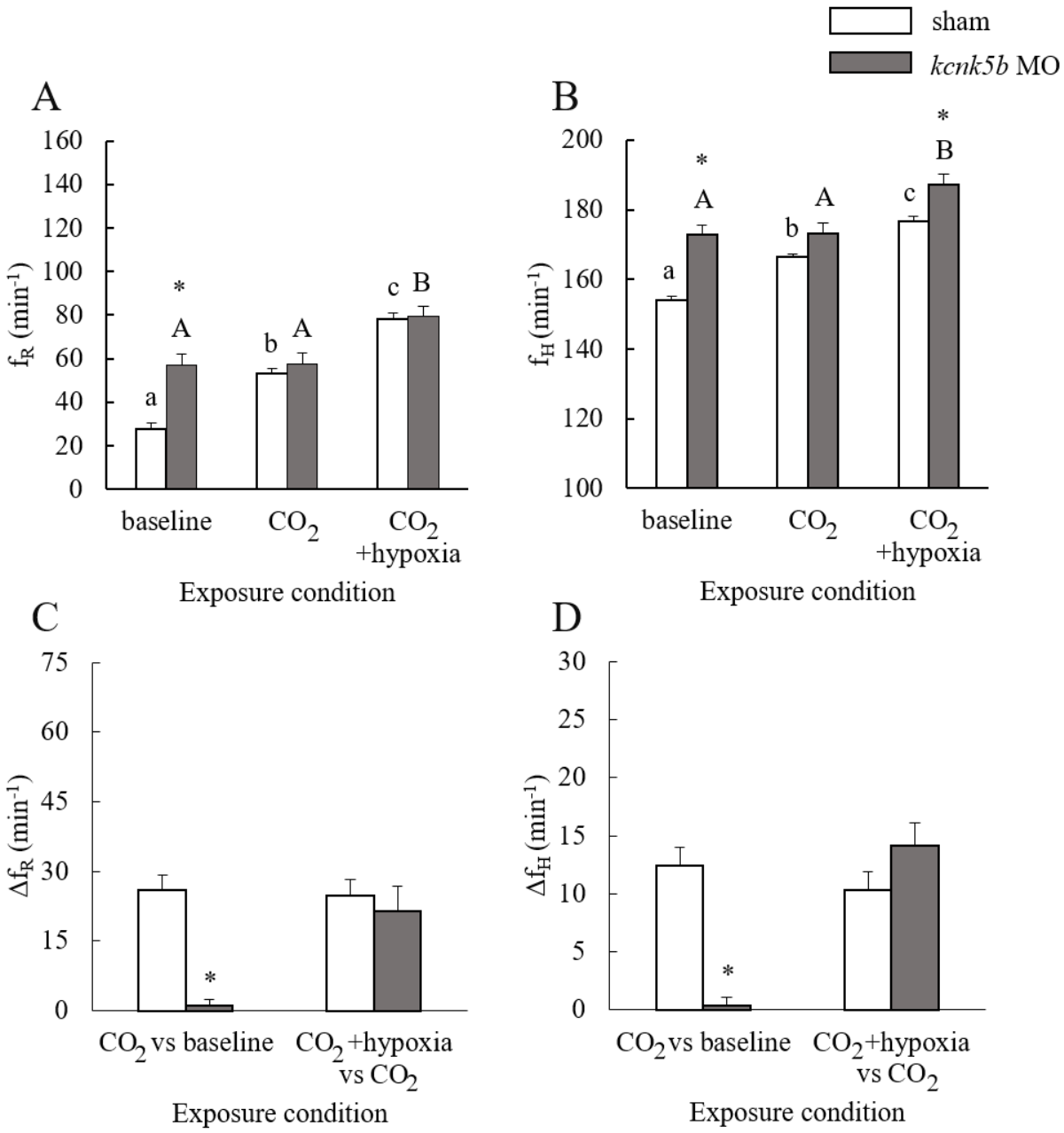
sham
kcnk5b MO
A
160
140
120
100
80
60
40
20
0
f_R (min^{-1})
a
A
b
A
c
B
*
baseline
CO_2
CO_2 +hypoxia
Exposure condition
B
200
180
160
140
120
100
f_H (min^{-1})
a
A
b
A
c
B
*
*
baseline
CO_2
CO_2 +hypoxia
Exposure condition
C
75
60
45
30
15
0
Δf_R (min^{-1})
*
CO_2 vs baseline
CO_2 +hypoxia vs CO_2
Exposure condition
D
30
25
20
15
10
5
0
Δf_H (min^{-1})
*
CO_2 vs baseline
CO_2 +hypoxia vs CO_2
Exposure condition

Figure 3.14: The effect of double knockdown of *kcnk5a* (using the translation-blocking morpholino) and *kcnk5b* (splice-blocking morpholino) on ventilation frequency (f_R; A) and heart rate (f_H; B) in 4 dpf zebrafish (*Danio rerio*) larvae exposed to normoxic normocapnia (baseline), hypercapnia (1.5% CO_2), or hypoxic (water O_2 tension of 30 mmHg) hypercapnia (1.5% CO_2). In panel A, a significant interaction between exposure condition and treatment group was detected (two-way RM ANOVA on reciprocal-transformed data, $P < 0.001$); bars that share a letter are not significantly different from one another and an asterisk indicates a significant difference between sham and morphant larvae. In panel B, a significant interaction between exposure condition and treatment group was detected (two-way RM ANOVA on ranks, $P = 0.017$); bars that share a letter are not significantly different from one another and an asterisk indicates a significant difference between sham and morphant larvae. The effect of double knockdown on changes in ventilation frequency (C) and heart rate (D) between exposure conditions also is presented. An asterisk indicates a significant difference between sham and double morphant larvae (for C, Student's *t*-test, $P = 0.000229$ and rank sum test, $P = 0.028$; for D, rank sum test, $P < 0.001$ and 0.442). Values are means + SEM, $N = 8$.

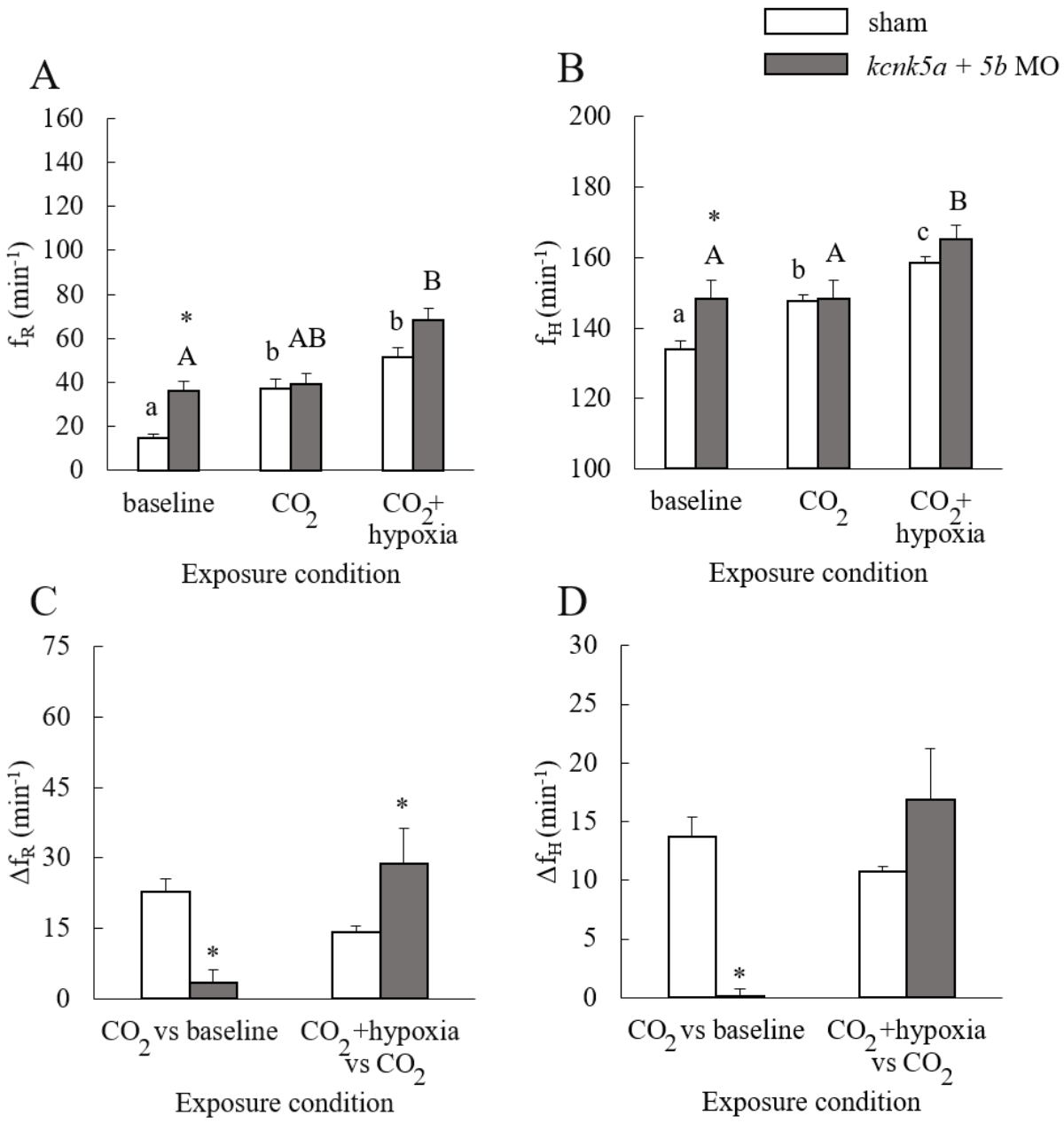
A
B
sham
kcnk5a + 5b MO
f_R (min^{-1})
f_H (min^{-1})
baseline
CO_2
CO_2+ hypoxia
Exposure condition
C
D
Δf_R (min^{-1})
Δf_H (min^{-1})
CO_2 vs baseline
CO_2 +hypoxia vs CO_2

Chapter 4: Discussion

4.1 Overview

The purpose of the current study was to localize TASK-2 channels in zebrafish and to determine whether one or both TASK-2 paralogues play a role in the CO_2 sensing pathway. Chemosensitive NECs have been found in all fish species studied to date (Perry and Tzaneva, 2016; Porteus et al., 2012) but the molecular sensor for CO_2 still has not been identified (Perry and Abdallah, 2012). NECs isolated from adult zebrafish gill tissue responded to increasing CO_2 levels through inhibition of a background K^+ channel (Qin et al., 2010); the present study investigated TASK-2 channels as a candidate for this background K^+ channel. The TASK-2 channel was of particular interest because studies have suggested that CO_2 can inhibit TASK-2 channels directly, and in addition TASK-2 channels exhibit direct sensitivity to intracellular and extracellular acidification (Peña-Münzenmayer et al., 2014). Because the work to date has used only *in vitro* approaches, the present study focused on localizing TASK-2 channels to NECs, and determining whether TASK-2 has a role in sensing CO_2 *in vivo.* The main findings of the current study are that TASK-2 appears to be expressed in NECs in the skin of zebrafish larvae and in the gill of adult fish, and that the cardiorespiratory response to hypercapnia is blunted in fish experiencing reduced expression of one or both TASK-2 paralogues. Therefore, the present study provides the first direct evidence that TASK-2 is present in the chemosensing cells of zebrafish, and that TASK-2 is a key component of the CO_2 sensing cascade that allows NECs to respond to hypercapnia.

4.2 Cardiorespiratory responses to hypercapnia in larval zebrafish

Larval (4 dpf) zebrafish of the present study responded to hypercapnia with increases in both ventilation frequency and heart rate. Miller et al. (2014) also reported tachycardia in response to hypercapnia in larval zebrafish, with the sensitivity to CO_2 increasing with increasing age. Whereas a significant tachycardia was observed in 7 dpf larvae at 0.5% CO_2, 5 dpf larvae required 0.75% CO_2 to mount a significant tachycardia and responses to the range of CO_2 tested (0.25-0.75% CO_2) were not significant in 4 dpf larvae (Miller et al., 2014). In the present study, a robust heart rate response was observed in 4 dpf larvae at 1.5% CO_2, in agreement with the notion that sensitivity to CO_2 increases with age. Whether this difference in responsiveness reflects age-dependent differences in the sensitivity of NECs to CO_2, or age-dependent differences in the efferent limb of the cardiac CO_2 chemoreflex, remains to be determined. Miller et al. (2014) reported that CO_2 itself rather than CO_2-induced changes in pH were responsible for the hypercapnia-induced tachycardia in zebrafish larvae – heart rate was decreased when water pH was lowered in the absence of CO_2. In addition, the CO_2-induced cardiac reflex was dependent upon cytosolic CA (Miller et al., 2014). In these respects, the cardiac response to hypercapnia resembles that observed in adult teleost fish, although in the species that have been tested to date (which do not include zebrafish), bradycardia rather than tachycardia is the typical response to hypercapnia (Perry and Gilmour, 2002).

In the present study, 4 dpf zebrafish larvae also responded to hypercapnia with an increase in breathing frequency, the first time to our knowledge that breathing responses to hypercapnia have been reported in developing fish. Breathing frequency was assessed on the basis of buccal or opercular movements, and as in previous studies (Coccimiglio and Jonz, 2012; Jonz and Nurse, 2005; Perry and Tzaneva, 2016; Porteus et al., 2015; Shakarchi et al., 2013), an increase in these movements was interpreted as a hyperventilatory response. Jonz and Nurse

(2005) reported that buccal and opercular movements appeared at ~3 dpf, and that also at 3 dpf, the response to hypoxia included a significant increase in the frequency of buccal and opercular movements. The buccal and opercular movements are presumed to benefit oxygen uptake, although whether the main benefit is to branchial or cutaneous oxygen uptake is unclear; zebrafish larvae can rely completely on cutaneous oxygen uptake until at least 7 dpf (Rombough, 2002). The increase in breathing frequency in response to hypercapnia in 4 dpf larval zebrafish contrasts with the hyperventilatory response to hypercapnia in adult fish, which consists of an increase in breathing amplitude in the absence of any effect on ventilation frequency (Vulesevic et al., 2006). In addition, adult zebrafish appear to be more sensitive to CO_2 than larval fish, with hyperventilation occurring at water CO_2 tensions as low as 0.13% CO_2 (1 mmHg) in adult fish (Vulesevic et al., 2006), whereas pilot trials suggested that 1.5% CO_2 was necessary to elicit reliable hyperventilatory responses in 4 dpf larval zebrafish. The increase in sensitivity of the ventilatory response to CO_2 with increasing age (larva vs adult) parallels the increasing sensitivity of the cardiac response to CO_2 (within larvae). The underlying basis of these changes in responsiveness warrants investigation.

4.3 Distribution of *kcnk5*/TASK-2 in larval zebrafish and adult zebrafish gill

In mice, TASK-2 expression has been localized to several regions within the brain, including the RTN, and strong expression has also been observed in renal proximal tubules and papillary collecting ducts of the kidney, where TASK-2 has been implicated in bicarbonate reabsorption (Gestreau et al., 2010; Warth et al., 2004; see also reviews by Cid et al., 2013; Lopez-Cayuqueo et al., 2015). Similarly, in the only previous localization of zebrafish TASK-2

paralogues, a tissue distribution at the mRNA level revealed the expression of *kcnk5a* and *kcnk5b* mRNA in a variety of tissues from adult fish, including gill, kidney, brain and eye (Perathoner et al., 2014). The findings of the present study allowed more specific localization of TASK-2 expression. In particular, the results indicate that TASK-2 is localized to NECs in the larval integument and adult gill. In addition, TASK-2 was observed on nerve varicosities in larval zebrafish. *In situ* hybridization revealed that *kcnk5a* mRNA is expressed in the epithelium surrounding the larval yolk sac, a site of high NEC abundance in larvae at 4 dpf (Coccimiglio and Jonz, 2012). A strong staining pattern for *kcnk5a* mRNA also was observed in the brain and eye region of larvae, in agreement with the tissue distribution study of Perathoner et al. (2014). To date there have been no studies of the specific location of TASK-2 at the protein level in zebrafish and therefore a key goal of the present study was to investigate TASK-2 protein expression using antibodies raised against peptides specific to zebrafish TASK-2 and TASK-2b proteins.

Immunolabelling of larvae and adult gill tissue with antibodies against TASK-2, 5-HT (as a marker for NECs; Bailly et al., 1992) and zn-12 (as a neuronal marker; Metcalfe *et al.* 1990) revealed co-expression of 5-HT and TASK-2 in a subset of NECs. In larvae, co-expression of TASK-2 and zn-12 was detected in varicosities along nerves, a pattern that was absent from adult gill tissue. In both larval and adult NECs, staining for TASK-2 was present in a faint ring-like pattern and this staining pattern was lost in larvae injected with either the splice-blocking or translation-blocking morpholino against TASK-2. This staining pattern is consistent with a membrane localization of TASK-2, the expected location for a membrane channel (Lesage, 2003). Because it was difficult to distinguish staining associated with the nerve from that associated with the NECs in larvae, performing immunohistochemistry on isolated cells would

be a useful approach. Also, this approach would allow comparisons of TASK-2 expression between larvae and adults. In the present study, stronger staining was observed in adult gill tissue than in larvae, but whether this reflects differences in TASK-2 expression between adult and larval zebrafish requires further investigation.

As a result of technical issues, the presence of *kcnk5b* mRNA in zebrafish larvae could not be investigated via *in situ* hybridization. Moreover, the results of immunohistochemistry experiments using a custom antibody raised against a zebrafish-specific TASK-2b peptide were inconclusive. In western analysis, use of the TASK-2b antibody identified a band of the appropriate size, but the staining seen with immunohistochemistry was not convincing. Thus, confirmation of TASK-2b expression in NECs of larval and adult zebrafish requires further work.

4.4 Effects of TASK-2 or TASK-2b knockdown on cardiorespiratory responses to hypercapnia

The present study provided the first investigation of the functional role of TASK-2 and TASK-2b in zebrafish *in vivo* by comparing the cardiorespiratory response to hypercapnia in sham-treated larvae with those in larvae experiencing knockdown of TASK-2 and/or TASK-2b. Overall, the results demonstrate that cardiorespiratory responses to hypercapnia are blunted in zebrafish larvae experiencing TASK-2 and/or TASK-2b knockdown, without an additive effect of double knockdown.

Knockdown of TASK-2 was effective at 4 dpf, as demonstrated by western blot analysis for larvae injected with the translation-blocking morpholino, and PCR analysis for larvae

injected with the splice-blocking morpholino. Specifically, western blot analysis revealed a significant decrease in the intensity of the band representing TASK-2 for larvae injected with the translation-blocking morpholino, i.e. reduced protein abundance. The effectiveness of the splice-blocking morpholino was investigated by RT-PCR and immunohistochemistry. Initially, exon-specific primers were used with the prediction being the absence of transcript in samples prepared from the *kcnk5a* morphant larvae because the splice-blocking morpholino binds to the first acceptor site of the pre-mRNA, leaving a long intron in the sequence that would be difficult to amplify by regular RT-PCR owing to the large size of the resulting mRNA. Unexpectedly, however, transcript was detected in samples prepared from *kcnk5a* morphant larvae. Antisense morpholino oligonucleotides are typically not completely effective and therefore splicing of a small amount of transcript can occur (Bill et al., 2009), which likely accounted for the detection of transcript in the morphant larvae. However, when using the exon-specific primers, transcript abundance was significantly greater in the sham-injected larvae compared to the morphant larvae, a result which is consistent with *kcnk5a* knockdown.

To further investigate the efficacy of knockdown, intron-specific primers were used. These primers should not yield an amplicon for samples prepared from sham-injected larvae because splicing occurs properly in this group of fish, but with samples prepared from the *kcnk5a* morphant larvae that retain the intron, an amplicon should be present. With the intron-specific primers, amplicons were obtained for both sham-treated and *kcnk5a* morpholino-injected larvae, although in lower abundance for the sham-injected larvae. Both pre-mRNA and mRNA can be isolated using standard total RNA isolation techniques (Evans-Molina et al., 2007), and use of random hexamer primers will generate cDNA from both types of mRNA. Moreover, rates of mRNA synthesis (3-4 kb min^{-1} in mammals, ~2 kb min^{-1} in insects and yeast) suggest that pre-

mRNA can be present in the cell long enough to be isolated (Darnell, 2013). Therefore, the intron-specific primers used in the present experiment may have detected pre-mRNA in sham-injected larvae, accounting for the presence of transcript. Collectively the data suggest that the splice-blocking morpholino was effective. With the exon-specific primers, transcript abundance was significantly greater in the sham-injected larvae compared to the morphant larvae, whereas with the intron-specific primers, transcript abundance was significantly greater in the *kcnk5a* morphant larvae than in the sham-injected larvae. In addition, immunohistochemistry revealed the absence of the TASK-2-specific ring-like staining surrounding the NEC in *kcnk5a* morphant larvae, indicating successful knockdown of TASK-2 protein levels. Similarly, knockdown of TASK-2b for the splice-blocking *kcnk5b* morpholino was effective at 4 dpf, as demonstrated by western blot and RT-PCR analyses. The smaller transcript expected as a result of the morpholino binding to a splice-acceptor site thus resulting in a shortened product was detected by RT-PCR, and in addition, western blot analysis showed that the band corresponding to TASK-2b was absent from *kcnk5b* morphant larvae.

Overall, similar patterns of change in resting breathing and heart rates and the responses to hypercapnia were elicited by TASK-2 or TASK-2b knockdown, although minor differences were apparent across experimental trials. Knockdown of TASK-2 using either a translation-blocking or a splice-blocking morpholino, and knockdown of TASK-2b using a splice-blocking morpholino, resulted in higher resting breathing and heart rates coupled with blunted responses to hypercapnia. The significant attenuation of ventilation and heart rate responses to hypercapnia were specific to this stimulus because morphant and sham-treated larvae responded with similar increases in ventilation and heart rate to a hypoxic stimulus. The responses to hypoxia as well as the similar effects of adrenaline on ventilation and heart rate between sham-treated and morphant

larvae indicated that morphant larvae retained the capacity to increase ventilation and heart rate, but did not do so in response to hypercapnia.

In mammals, elimination of TASK-2 results in RTN neurons with an elevated (depolarized) resting membrane potential (Wang et al., 2013) and mice that exhibit reduced ventilatory responses to relatively high CO_2 tensions (Gestreau et al., 2010). Background potassium channels such as TASK-2 are involved with maintaining the resting membrane potential in cells. When these channels are absent, the resting membrane potential of the cell increases, thus becoming more depolarized. This higher resting membrane potential, in turn, results in more frequent firing (Lesage, 2003). Ventilatory responses to CO_2/pH reflect the intrinsic pH sensitivity of the TASK-2 channel – in the absence of this channel, the central respiratory chemoreflex in mice is reduced by ~65% (Guyenet et al., 2016). Taking into account the differences between mammals, which exhibit a central CO_2 ventilatory drive, and fish, in which ventilation is driven primarily by O_2 via peripheral chemoreceptors, with a role for CO_2 detected by peripheral chemoreceptors, the findings of the present study for morphant zebrafish larvae with reduced TASK-2 or TASK-2b expression demonstrated strong parallels with TASK-2 knockout mice. In zebrafish larvae experiencing reduced TASK-2 or TASK-2b expression, resting ventilation and heart rate were elevated, a finding that is consistent with TASK-2 or TASK-2b contributing to resting membrane potential. If reduced expression of this channel results in depolarization of the resting membrane potential of NECs, as in RTN neurons of TASK-2 knockout mice (Wang et al., 2013), then elevated NEC activity in turn could drive increased resting ventilation and heart rate in morphant zebrafish larvae. Zebrafish TASK-2, like mouse TASK-2, exhibits inherent sensitivity to intracellular pH, extracellular pH and CO_2 (Peña-Münzenmayer et al., 2014). Reduced expression of TASK-2 or TASK-2b blunted

cardiorespiratory responses to hypercapnia in morphant zebrafish, a finding that is consistent with the hypothesis that CO_2 sensing in zebrafish NECs relies on the sensitivity of TASK-2 and/or TASK-2b to CO_2/pH. The similarity of responses to knockdown of either TASK-2 or TASK-2b suggests that these paralogues play comparable roles in CO_2 sensing in zebrafish. In addition, the absence of additive effects of double knockdown of TASK-2 and TASK-2b together indicates that loss of either TASK-2 or TASK-2b is sufficient to impair the CO_2 sensing pathway.

Although there were clear similarities in the responses to TASK-2 or TASK-2b knockdown across the experimental trials, there were also differences, largely in whether a response achieved statistical significance. These minor discrepancies may be attributed at least in part to differences in sample sizes and hence statistical power between trials. The translation-blocking and splice-blocking *kcnk5a* morpholinos had different modes of action but caused similar effects (i.e. a reduction in TASK-2 expression), and yielded similar responses at the whole-animal level, strengthening confidence in the impact of TASK-2 knockdown on cardiorespiratory responses. Collectively, the data support a role for TASK-2 paralogues in CO_2 sensing in zebrafish larvae. More specifically, the finding of the present study suggest that TASK-2 serves as the background K^+ channel in NECs that closes in response to CO_2 and/or pH (Qin et al., 2010), leading to membrane depolarization, a rise in intracellular Ca^{2+} levels (Abdallah et al., 2015), release of neurotransmitter and ultimately, the cardiorespiratory responses observed in larval and adult zebrafish.

References

Abdallah, S. J., Jonz, M. G. and Perry, S. F. (2015). Extracellular H^+ induces Ca^{2+} signals in respiratory chemoreceptors of zebrafish. *Pflügers Arch. - Eur. J. Physiol.* **467**, 399–413.

Ahmad, H. R. and Loeschcke, H. H. (1982). Transient and steady state responses of pulmonary ventilation to the medullary extracellular pH after approximately rectangular changes in alveolar PCO2. *Pflugers Arch.* **395**, 285–92.

Bailly, Y., Dunel-Erb, S. and Laurent, P. (1992). The Neuroepithelial Cells of the Fish Gill Filament: Indolamine-lmmunocytochemistry and Innervation. *Anat. Rec.* **233**, 143–161.

Bayliss, D. A., Talley, E. M., Sirois, J. E. and Lei, Q. (2001). TASK-1 is a highly modulated pH-sensitive "leak" K^+ channel expressed in brainstem respiratory neurons. *Respir. Physiol.* **129**, 159–174.

Bill, B. R., Petzold, A. M., Clark, K. J., Schimmenti, L. A. and Ekker, S. C. (2009). A Primer for Morpholino Use in Zebrafish. *Zebrafish* **6**, 69–77.

Buckler, K. J. (1999). Background leak K^+-currents and oxygen sensing in carotid body type 1 cells. *Respir. Physiol.* **115**, 179–187.

Buckler, K. J. (2007). TASK-like potassium channels and oxygen sensing in the carotid body. *Respir. Physiol. Neurobiol.* **157**, 55–64.

Buckler, K. J. (2015). TASK channels in arterial chemoreceptors and their role in oxygen and acid sensing. *Pflugers Arch.* **467**, 1013–25.

Buckler, K. J. and Vaughan-Jones, R. D. (1993). Effects of acidic stimuli on intracellular calcium in isolated type I cells of the neonatal rat carotid body. *Pflugers Arch.* **425**, 22–7.

Buckler, K. J. and Vaughan-Jones, R. D. (1994). Effects of hypercapnia on membrane potential and intracellular calcium in rat carotid body type I cells. *J. Physiol.* 157–71.

Buckler, K. J., Williams, B. A. and Honore, E. (2000). An oxygen-, acid- and anaesthetic-sensitive TASK-like background potassium channel in rat arterial chemoreceptor cells. *J. Physiol.* **525**, 135–142.

Burleson, M. L. and Smatresk, N. J. (2000). Branchial chemoreceptors mediate ventilatory responses to hypercapnic acidosis in channel catfish. *Comp. Biochem. Physiol. A. Mol. Integr. Physiol.* **125**, 403–14.

Burleson, M. L., Mercer, S. E. and Wilk-Blaszczak, M. A. (2006). Isolation and characterization of putative O2 chemoreceptor cells from the gills of channel catfish (*Ictalurus punctatus*). *Brain Res.* **1092**, 100–107.

Carrie, D. W. and Gilmour, K. M. (2012). Intracellular carbonic anhydrase contributes to the red blood cell adrenergic response in rainbow trout *Oncorhynchus mykiss*. *Respir. Physiol. Neurobiol.* **184**, 60–64.

Cid, L. P., Roa-Rojas, H. A., Niemeyer, M. I., González, W., Araki, M., Araki, K. and

Sepúlveda, F. V. (2013). TASK-2: a K_2P K^+ channel with complex regulation and diverse physiological functions. *Front. Physiol.* **4**, 1-9.

Coccimiglio, M. L. and Jonz, M. G. (2012). Serotonergic neuroepithelial cells of the skin in developing zebrafish: morphology, innervation and oxygen-sensitive properties. *J. Exp. Biol.* **215**, 3881–3894.

Coolidge, E. H., Ciuhandu, C. S. and Milsom, W. K. (2008). A comparative analysis of putative oxygen-sensing cells in the fish gill. *J. Exp. Biol.* **211**, 1231–1242.

Crocker, C. E., Farrell, A. P., Gamperl, A. K., Cech, J. J., Carlos, E. and Kurt, A. (2000). Cardiorespiratory responses of white sturgeon to environmental hypercapnia. *Am. J. Physiol. Regul. Integr. Comp. Physiol.* **8751**, R617–R628.

Cutz, E., Speirs, V., Yeger, H., Newman, C., Wang, D. and Perrin, D. G. (1993). Cell biology of pulmonary neuroepithelial bodies. Validation of an in vitro model. I. Effects of hypoxia and Ca^{2+} ionophore on serotonin content and exocytosis of dense core vesicles. *Anat. Rec.* **236**, 41–52.

Darnell, J. E. and Jr. (2013). Reflections on the history of pre-mRNA processing and highlights of current knowledge: a unified picture. *RNA* **19**, 443–60.

Dunel-Erb, S., Bailly, Y. and Laurent, P. (1982). Neuroepithelial cells in fish gill primary lamellae. *J. Appl. Physiol.* **53**, 1342–53.

Enyedi, P. and Czirják, G. (2010). Molecular background of leak K^+ currents: two-pore domain potassium channels. *Physiol. Rev.* **90**, 559–605.

Evans-Molina, C., Garmey, J. C., Ketchum, R., Brayman, K. L., Deng, S. and Mirmira, R. G. (2007). Glucose regulation of insulin gene transcription and pre-mRNA processing in human islets. *Diabetes* **56**, 827–35.

Feldman, J. L., Mitchell, G. S. and Nattie, E. E. (2003). Breathing: rhythmicity, plasticity, chemosensitivity. *Annu. Rev. Neurosci.* **26**, 239–266.

Gestreau, C., Heitzmann, D., Thomas, J., Dubreuil, V., Bandulik, S., Reichold, M., Bendahhou, S., Pierson, P., Sterner, C., Peyronnet-Roux, J., et al. (2009). TASK-2 potassium channels set central respiratory CO_2 and O_2 sensitivity. *Proc. Natl. Acad. Sci. U. S. A.* **107**, 2325–30.

Gilmour, K. M. (2001). The CO_2/pH ventilatory drive in fish. *Comp. Biochem. Physiol. Part A* **130**, 219–240.

Gilmour, K. and Perry, S. (1994). The effects of hypoxia, hyperoxia or hypercapnia on the acid-base disequilibrium in the arterial blood of rainbow trout. *J. Exp. Biol.* **192**, 269-84.

Gilmour, K. M. and Perry, S. F. (2007). Branchial chemoreceptor regulation of cardiorespiratory function. *Fish Physiol.* **25**, 97–151.

Gilmour, K. M., Milsom, W. K., Rantin, F. T., Reid, S. G. and Perry, S. F. (2005). Cardiorespiratory responses to hypercarbia in tambaqui *Colossoma macropomum*: chemoreceptor orientation and specificity. *J. Exp. Biol.* **208**, 1095-107.

Goldstein, S. a N., Bayliss, D. a, Kim, D., Lesage, F. and Plant, L. D. (2005). International Union of Pharmacology. LV. Nomenclature andmolecular relationships of two-P potassium channels. *Pharmacol. Rev.* **57**, 527–540.

Goniakowska-Witalińska, L., Zaccone, G., Fasulo, S., Mauceri, A., Licata, A. and Youson, J. (1995). Neuroendocrine cells in the gills of the bowfin *Amia calva*. An ultrastructural and immunocytochemical study. *Folia Histochem. Cytobiol.* **33**, 171–7.

Gonzalez, C., Almaraz, L., Obeso, A. and Rigual, R. (1994). Carotid Body Chemoreceptors: From Natural to Sensory Discharges. *Physiol. Rev.* **74**, 829–877.

Guyenet, P. G., Stornetta, R. L. and Bayliss, D. A. (2008). Retrotrapezoid nucleus and central chemoreception. *J. Physiol.* **586**, 2043–2048.

Guyenet, P. G., Bayliss, D. A., Stornetta, R. L., Ludwig, M.-G., Kumar, N. N., Shi, Y., Burke, P. G. R., Kanbar, R., Basting, T. M., Holloway, B. B., et al. (2016). Proton detection and breathing regulation by the retrotrapezoid nucleus. *J. Physiol.* **594**, 1529–51.

Hirata, Y. and Oku, Y. (2010). TRP channels are involved in mediating hypercapnic Ca^{2+} responses in rat glia-rich medullary cultures independent of extracellular pH. *Cell Calcium* **48**, 124–132.

Hockman, D., Burns, A., Schlosser, G., Gates, K. P., Jevans, B., Mongera, A., Fisher, S., Unlu, G., Knapik, E. W., Kaufman, C. K., et al. (2017). Evolution of the hypoxia-sensitive cells involved in amniote respiratory reflexes. *Elife* **6**, e21231.

Jonz, M. G. and Nurse, C. A. (2003). Neuroepithelial cells and associated innervation of the zebrafish gill: A confocal immunofluorescence study. *J. Comp. Neurol.* **461**, 1–17.

Jonz, M. G. and Nurse, C. A. (2005). Development of oxygen sensing in the gills of zebrafish. *J. Exp. Biol.* **208**, 1537–1549.

Jonz, M. G. and Nurse, C. A. (2006). Ontogenesis of oxygen chemoreception in aquatic vertebrates. *Respir. Physiol. Neurobiol.* **154**, 139–152.

Jonz, M. G., Fearon, I. M. and Nurse, C. A. (2004). Neuroepithelial oxygen chemoreceptors of the zebrafish gill. *J. Physiol.* **560**, 737–752.

Jonz, M. G., Zachar, P. C., Da Fonte, D. F. and Mierzwa, A. S. (2015). Peripheral chemoreceptors in fish: A brief history and a look ahead. *Comp. Biochem. Physiol. Part A Mol. Integr. Physiol.* **186**, 27–38.

Kim, D., Cavanaugh, E. J., Kim, I. and Carroll, J. L. (2009). Heteromeric TASK-1/TASK-3 is the major oxygen-sensitive background K^+ channel in rat carotid body glomus cells. *J. Physiol.* **587**, 2963–75.

Kimmel, C. B., Ballard, W. W., Kimmel, S. R., Ullmann, B. and Schilling, T. F. (1995). Stages of Embryonic Development of the Zebrafish. *Dev. Dyn.* **10**, 253–310.

Kumar, P. and Bin-Jaliah, I. (2007). Adequate stimuli of the carotid body: More than an oxygen sensor? *Respir. Physiol. Neurobiol.* **157**, 12–21.

Kumar, P. and Prabhakar, N. R. (2012). Peripheral chemoreceptors: Function and plasticity of

the carotid body. *Compr. Physiol.* **2**, 141–219.

Kumar, N. N., Velic, A., Soliz, J., Shi, Y., Li, K., Wang, S., Weaver, J. L., Sen, J., Abbott, S. B. G., Lazarenko, R. M., et al. (2015). Regulation of breathing by CO_2 requires the proton-activated receptor GPR4 in retrotrapezoid nucleus neurons. *Science*. **348**, 1255-1260.

Lahiri, S. and Forster, R. E. (2003). CO_2/H^+ sensing: peripheral and central chemoreception. *Int. J. Biochem. Cell Biol.* **35**, 1413–1435.

Lesage, F. (2003). Pharmacology of neuronal background potassium channels. *Neuropharmacology* **44**, 1–7.

Lesage, F., Guillemare, E., Fink, M., Duprat, F., Lazdunski, M., Romey, G. and Barhanin, J. (1996). TWIK-1, a ubiquitous human weakly inward rectifying K^+ channel with a novel structure. *EMBO J.* **15**, 1004–11.

Lopez-Cayuqueo, K. I., Pena-Munzenmayer, G., Niemeyer, M. I., Sepulveda, F. V. and Cid, L. P. (2015). TASK-2 K_2P K^+ channel: thoughts about gating and its fitness to physiological function. *Pflugers Arch. Eur. J. Physiol.* **467**, 1043–1053.

McKendry, J. E. and Perry, S. F. (2001). Cardiovascular effects of hypercarbia in rainbow trout (*Oncorhynchus mykiss*): a role for externally oriented chemoreceptors. *J. Exp. Biol.* **204**, 115–25.

McKendry, J. E., Milsom, W. K. and Perry, S. F. (2001). Branchial CO_2 receptors and cardiorespiratory adjustments during hypercarbia in pacific spiny dogfish (*Squalus acanthias*). *J. Exp. Biol.* 1519–1527.

Metcalfe, W. K., Myers, P. Z., Trevarrow, B., Bass, M. B. and Kimmel, C. B. (1990). Primary neurons that express the L2/HNK-1 carbohydrate during early development in the zebrafish. *Development.* **110**, 491-504.

Miller, S., Pollack, J., Bradshaw, J., Kumai, Y. and Perry, S. F. (2014). Cardiac responses to hypercapnia in larval zebrafish (*Danio rerio*): the links between CO_2 chemoreception, catecholamines and carbonic anhydrase. *J. Exp. Biol.* **217**, 3569–78.

Milsom, W. K. (2002). Phylogeny of CO_2/H^+ chemoreception in vertebrates. *Respir. Physiol. Neurobiol.* **131**, 29–41.

Milsom, W. K., Reid, S. G., Rantin, F. T. and Sundin, L. (2002). Extrabranchial chemoreceptors involved in respiratory reflexes in the neotropical fish *Colossoma macropomum* (the tambaqui). *J. Exp. Biol.* **205**, 1765–1774.

Mulkey, D. K., Stornetta, R. L., Weston, M. C., Simmons, J. R., Parker, A., Bayliss, D. A. and Guyenet, P. G. (2004). Respiratory control by ventral surface chemoreceptor neurons in rats. *Nat. Neurosci.* **7**, 1360–1369.

Mulkey, D. K., Talley, E. M., Stornetta, R. L., Siegel, A. R., West, G. H., Chen, X., Sen, N., Mistry, A. M., Guyenet, P. G. and Bayliss, D. A. (2007). TASK channels determine pH sensitivity in select respiratory neurons but do not contribute to central respiratory chemosensitivity. *J. Neurosci.* **27**, 14049–14058.

Niemeyer, M. I., González-Nilo, F. D., Zúñiga, L., González, W., Cid, L. P. and Sepúlveda, F. V (2007). Neutralization of a single arginine residue gates open a two-pore domain, alkali-activated K^+ channel. *Proc. Natl. Acad. Sci. U. S. A.* **104**, 666–71.

Niemeyer, M. I., Cid, L. P., Peña-Münzenmayer, G. and Sepúlveda, F. V (2010). Separate gating mechanisms mediate the regulation of K_2P potassium channel TASK-2 by intra- and extracellular pH. *J. Biol. Chem.* **285**, 16467–75.

Nurse, C. A. (2014). Synaptic and paracrine mechanisms at carotid body arterial chemoreceptors. *J. Physiol.* **16**, 3419–3426.

Nurse, C. A. and Piskuric, N. A. (2013). Signal processing at mammalian carotid body chemoreceptors. *Semin. Cell Dev. Biol.* **24**, 22–30.

Ortega-Sáenz, P., Pardal, R., Levitsky, K., Villadiego, J., Muñoz-Manchado, A. B., Durán, R., Bonilla-Henao, V., Arias-Mayenco, I., Sobrino, V., Ordóñez, A., et al. (2013). Cellular properties and chemosensory responses of the human carotid body. *J. Physiol.* **591**, 6157–73.

Peña-Münzenmayer, G., Niemeyer, M. I., Sepúlveda, F. V and Cid, L. P. (2014). Zebrafish and mouse TASK-2 K^+ channels are inhibited by increased CO_2 and intracellular acidification. *Pflugers Arch.* **466**, 1317–27.

Peng, Y.-J., Nanduri, J., Raghuraman, G., Souvannakitti, D., Gadalla, M. M., Kumar, G. K., Snyder, S. H. and Prabhakar, N. R. (2010). H_2S mediates O_2 sensing in the carotid body. *Proc. Natl. Acad. Sci. U. S. A.* **107**, 10719–10724.

Perathoner, S., Daane, J. M., Henrion, U., Seebohm, G., Higdon, C. W., Johnson, S. L., Nüsslein-Volhard, C. and Harris, M. P. (2014). Bioelectric signaling regulates size in zebrafish fins. *PLoS Genet.* **10**, 1-11.

Perry, S. F. and Abdallah, S. (2012). Mechanisms and consequences of carbon dioxide sensing in fish. *Respir. Physiol. Neurobiol.* **184**, 309–15.

Perry, S. F. and Gilmour, K. M. (1996). Consequences of catechilamine release on ventilation and blood oxygen transport during hypoxia and hypercapniain an elasmobranch (*Squalus acanthias*) and a teleost (*Oncorhynchum mykiss*). *J. Exp. Biol.* 2105–2118.

Perry, S. F. and Gilmour, K. M. (2002). Sensing and transfer of respiratory gases at the fish gill. In *Journal of Experimental Zoology*, pp. 249–263.

Perry, S. F. and Mckendry, J. E. (2001). The relative roles of external and internal CO^2 versus H^+ in eliciting the cardiorespiratory responses of *Salmo salar* and *Squalus acanthias* to hypercarbia. *J. Exp. Biol.* 3963–3971.

Perry, S. F. and Reid, S. G. (2002). Cardiorespiratory adjustments during hypercarbia in rainbow trout *Oncorhynchus mykiss* are initiated by external CO_2 receptors on the first gill arch. *J. Exp. Biol.* **205**, 3357–65.

Perry, S. F. and Tzaneva, V. (2016). The sensing of respiratory gases in fish: Mechanisms and signalling pathways. *Respir. Physiol. Neurobiol.*

Perry, S. F., Fritsche, R., Hoagland, T. M., Duff, D. W. and Olson, K. R. (1999). The control of blood pressure during external hypercpnia in the rainbow trout *(Oncorhynchus mykiss)*. *J. Exp. Biol.* 2177–2190.

Perry, S. F., Jonz, M. G. and Gilmour, K. M. (2009). Oxygen Sensing And The Hypoxic Ventilatory Response. In *Fish Physiology*. 193–253.

Perry, S. F., Vulesevic, B., Braun, M. and Gilmour, K. M. (2009). Ventilation in Pacific hagfish (*Eptatretus stoutii*) during exposure to acute hypoxia or hypercapnia. *Respir. Physiol. Neurobiol.* **167**, 227–34.

Porteus, C. S., Brink, D. L. and Milsom, W. K. (2012). Neurotransmitter profiles in fish gills: Putative gill oxygen chemoreceptors. *Respir. Physiol. Neurobiol.* **184**, 316–325.

Porteus, C. S., Wright, P. a and Milsom, W. K. (2014). Characterisation of putative oxygen chemoreceptors in bowfin (*Amia calva*). *J. Exp. Biol.* **217**, 1269–77.

Porteus, C. S., Pollack, J., Tzaneva, V., Kwong, R. W. M., Kumai, Y., Abdallah, S. J., Zaccone, G., Lauriano, E. R., Milsom, W. K. and Perry, S. F. (2015). A role for nitric oxide in the control of breathing in zebrafish (*Danio rerio*). *J. Exp. Biol.* **218**, 3746-3753.

Putnam, R. W., Filosa, J. A. and Ritucci, N. A. (2004). Cellular mechanisms involved in CO_2 and acid signaling in chemosensitive neurons. *Am. J. Physiol. Cell Physiol.* **287**, C1493-526.

Qin, Z., Lewis, J. E. and Perry, S. F. (2010). Zebrafish (*Danio rerio*) gill neuroepithelial cells are sensitive chemoreceptors for environmental CO_2. *J. Physiol.* **588**, 861–72.

Randall, D. (1982). The Control of Respiration and Circulation in Fish During Exercise and Hypoxia. *J. Exp. Biol.* 275–288.

Rantin, F. T., Kalinin, A. L., Glass, M. L. and Fernandes, M. N. (1992). Respiratory responses to hypoxia in relation to mode of life of two erythrinid species (*Hoplias malabaricus* and *Hoplias lacerdae*). *J. Fish Biol.* **41**, 805–812.

Reid, S. G., Sundin, L., Kalinin, A. L., Rantin, F. T. and Milsom, W. K. (2000). Cardiovascular and respiratory reflexes in the tropical fish, traira *(Hoplias malabaricus)*: CO_2/pH chemoresponses. *Respir. Physiol.* **120**, 47–59.

Reyes, R., Duprat, F., Lesage, F., Fink, M., Farman, N. and Lazdunski, M. (1998). Cloning and expression of a novel pH-sensitive two pore domain potassium channel from human kidney. *J. Biol. Chem.* **273**, 30863–30869.

Rombough, P. (2002). Gills are needed for ionoregulation before they are needed for O_2 uptake in developing zebrafish, *Danio rerio*. *J. Exp. Biol.* **205**, 1787–1794.

Saltys, H., Jonz, M. and Nurse, C. (2006). Comparative study of gill neuroepithelial cells and their innervation in teleosts and Xenopus tadpoles. *Cell Tissue Res.* **323**, 1–10.

Sato, M. (1994). Effects of CO_2, acetate and lowering extracellular pH on cytosolic Ca^{2+} and pH in cultured glomus cells of the newborn rabbit carotid body. *Neurosci. Lett.* **173**, 159–62.

Severson, C. A., Wang, W., Pieribone, V. A., Dohle, C. I. and Richerson, G. B. (2003).

Midbrain serotonergic neurons are central pH chemoreceptors. *Nat. Neurosci.* **6**, 1139–1140.

Shakarchi, K., Zachar, P. C. and Jonz, M. G. (2013). Serotonergic and cholinergic elements of the hypoxic ventilatory response in developing zebrafish. *J. Exp. Biol.* **216**, 869-80.

Smith, F. M. and Jones, D. R. (1982). The effect of changes in blood oxygen-carrying capacity on ventilation volume in the rainbow trout (*Salmo gairdneri*). *J. Exp. Biol.* **97**, 325-334.

Smith, C. A., Rodman, J. R., Chenuel, B. J. A., Henderson, K. S. and Dempsey, J. A. (2006). Response time and sensitivity of the ventilatory response to CO_2 in unanesthetized intact dogs: central vs. peripheral chemoreceptors. *J Appl Physiol* **100**, 13–19.

Soncini, R. and Glass, M. L. (2000). Oxygen and acid-base status related drives to gill ventilation in carp. *J. Fish Biol.* **56**, 528–541.

Summers, B. A., Overholt, J. L., Prabhakar, N. R., Imber, A. N., Putnam, R. W., Huckstepp, R. T. R., Dale, N., Bihi, R., Eason, R., Spyer, K. M., et al. (2002). CO_2 and pH Independently Modulate L-Type Ca^{2+} Current in Rabbit Carotid Body Glomus Cells CO_2 and pH Independently Modulate L-Type Ca^{2+} Current in Rabbit Carotid Body Glomus Cells. *J. Neurophysiol.* **88**, 604–612.

Sundin, L., Reid, S. G., Rantin, F. T. and Milsom, W. K. (2000). Branchial Receptors and Cardiorespiratory Reflexes in a neotropical fish, the tambqui (*Colossoma macropomum*). *J. Exp. Biol.* 1225–1239.

Sundin, L., Burleson, M. L., Sanchez, A. P., Amin-Naves, J., Kinkead, R., Gargaglioni, L. H., Hartzler, L. K., Wiemann, M., Kumar, P. and Glass, M. L. (2007). Respiratory chemoreceptor function in vertebrates - Comparative and evolutionary aspects. *Integr. Comp. Biol.* **47**, 592–600.

Talley, E. M., Sirois, J. E., Lei, Q. and Bayliss, D. A. (2003). Two-Pore-Domain (Kcnk) Potassium Channels: Dynamic Roles in Neuronal Function. *Neurosci.* **9**, 46–56.

Tan, Z.-Y., Lu, Y., Whiteis, C. A., Benson, C. J., Chapleau, M. W. and Abboud, F. M. (2007). Acid-Sensing Ion Channels Contribute to Transduction of Extracellular Acidosis in Rat Carotid Body Glomus Cells. *Circ. Res.* **101**, 1009–1019.

Turner, P. J. and Buckler, K. J. (2013). Oxygen and mitochondrial inhibitors modulate both monomeric and heteromeric TASK-1 and TASK-3 channels in mouse carotid body type-1 cells. *J. Physiol.* **591**, 5977–98.

Vulesevic, B., McNeill, B. and Perry, S. F. (2006). Chemoreceptor plasticity and respiratory acclimation in the zebrafish *Danio rerio*. *J. Exp. Biol.* **209**, 1261–73.

Wang, S., Benamer, N., Zanella, S., Kumar, N. N., Shi, Y., Bévengut, M., Penton, D., Guyenet, P. G., Lesage, F., Gestreau, C., et al. (2013). TASK-2 channels contribute to pH sensitivity of retrotrapezoid nucleus chemoreceptor neurons. *J. Neurosci.* **33**, 16033–44.

Warth, R., Barrière, H., Meneton, P., Bloch, M., Thomas, J., Tauc, M., Heitzmann, D., Romeo, E., Verrey, F., Mengual, R., et al. (2004). Proximal renal tubular acidosis in TASK-2 K^+ channel-deficient mice reveals a mechanism for stabilizing bicarbonate

transport. *Proc. Natl. Acad. Sci. U. S. A.* **101**, 8215–20.

Washburn, C. P., Sirois, J. E., Talley, E. M., Guyenet, P. G. and Bayliss, D. a (2002). Serotonergic raphe neurons express TASK channel transcripts and a TASK-like pH- and halothane-sensitive K^+ conductance. *J. Neurosci.* **22**, 1256–1265.

Washburn, C. P., Bayliss, D. A. and Guyenet, P. G. (2003). Cardiorespiratory neurons of the rat ventrolateral medulla contain TASK-1 and TASK-3 channel mRNA. *Respir. Physiol. Neurobiol.* **138**, 19–35.

Westerfield, M. (2000). *The Zebrafish Book. A Guide for the Laboratory Use of Zebrafish (Danio rerio)*, 4th ed. Eugene: University of Oregon Press.

Williams, B. A. and Buckler, K. J. (2004). Biophysical properties and metabolic regulation of a TASK-like potassium channel in rat carotid body type 1 cells. *AJP Lung Cell. Mol. Physiol.* **286**, L221-30.

Zaccone, G., Tagliafierro, G., Fasulo, S., Ainis, L. and Mauceri, A. (1989). Histochemis Serotonin-like immunoreactive cells in the pulmonary epithelium of ancient fish species. *Histochemistry* **92**, 61–63.

Zaccone, G., Lauweryns, J. M., Fasulo, S., Tagliafierro, G., Ainis, L. and Licata, A. (1992). Immunocytochemical Localization of Serotonin and Neuropeptides in the Neuroendocrine Paraneurons of Teleost and Lungfish Gills. *Acta Zool.* **73**, 177–183.

Zaccone, G., Fasulo, S., Ainis, L. and Licata, A. (1997). Paraneurons in the Gills and Airways of Fishes. *Microsc. Res. Tech.* **12**, 4–12.

Zaccone, G., Mauceri, A. and Fasulo, S. (2006). Neuropeptides and Nitric Oxide Synthase in the Gill and the Air-breathing Organs of Fishes. *J. Exp. Zool.* **305A**, 428–439.

Zachar, P. C. and Jonz, M. G. (2012). Neuroepithelial cells of the gill and their role in oxygen sensing. *Respir. Physiol. Neurobiol.* **184**, 301–308.

Zhang, L., Nurse, C. a, Jonz, M. G. and Wood, C. M. (2011). Ammonia sensing by neuroepithelial cells and ventilatory responses to ammonia in rainbow trout. *J. Exp. Biol.* **214**, 2678–2689.